Third-order nonlinear time domain probes of solvation dynamics

Taiha Joo, Yiwei Jia, Jae-Young Yu, Matthew J. Lang, and Graham R. Fleming
Department of Chemistry and the James Franck Research Institute, The University of Chicago, Chicago, Illinois 60637

(Received 9 November 1995; accepted 22 January 1996)

Several closely related third-order nonlinear time-resolved spectroscopic techniques, pump/probe transient absorption, transient grating, and three pulse stimulated photon echo peak shift measurements, are investigated theoretically and experimentally. It is shown in detail, through the consideration of response functions and numerical simulations including both finite pulse durations and detuning from exact resonance, how the solvation dynamics are manifested in these third-order nonlinear time-resolved spectroscopies. It is shown that the three pulse stimulated photon echo peak shift measurement and the transient grating measurement can give accurate dynamical information, whereas transient absorption may not be a reliable technique for a study of solvation dynamics in some cases. The contribution of very slow or static (inhomogeneous) components to the dynamics, however, can only be obtained from the three pulse echo peak shift measurements. Comprehensive experimental measurements are presented to illustrate and corroborate the calculations. We show that it is possible to separate the intramolecular vibrational and solvent contributions to the dephasing (or optical lineshape). Furthermore it is shown that the solvation of polar solutes in polar protic solvents has rather universal characteristics. The initial ultrafast process, usually identified as an inertial response of solvent molecules, occurs on a ~100 fs time scale, and is essentially identical in methanol, ethanol, and butanol. The amplitude of this ultrafast component does, however, decrease with increasing alcohol size in 1-alkanols. The diffusive (>0.5 ps) regime of the solvation process shows a strong solvent dependence, and may be described satisfactorily by dielectric relaxation theories. [S0021-9606(96)02716-0]

I. INTRODUCTION

Solvent dynamics plays a crucial role in many chemical and physical processes in the condensed phases. In particular, the effects of solvation on the rate of electron transfer have been under intense study.[1–15] Recently, there has been substantial progress in understanding the dynamics in liquids as a result of both theoretical[16–27] and experimental[16,28–35] advances, especially for the latter in the time domain. In liquids, the environment of a chromophore (either a solvent molecule in a pure liquid or a solute molecule in a solution) fluctuates on a wide range of time scales, ranging from ~100 fs to nanoseconds and beyond.[36–38] Inertial behavior of the solvent molecules is usually invoked for the initial ultrafast process occurring on a 100 fs time scale,[16–24] and it may significantly influence the outcome of chemical reactions.

To fully characterize the dynamics, and thereby to obtain the dynamical spectrum of a system[39] or vice versa, one needs to know the amplitudes of the fluctuations as well as the time scales of each process. An optical absorption spectrum serves as an important probe for the dynamics. However, to characterize the time scales, one needs to turn to nonlinear spectroscopies. The third-order nonlinearity is the lowest-order nonzero nonlinear term in isotropic media, and nonlinear optical measurements have almost always exploited the third-order nonlinearity. Recently, studies utilizing higher-order nonlinear terms are starting to appear. The third-order nonlinear term involves three field-matter interactions and thus most of the pump/probe type time domain measurements, where the pump pulse interacts twice with the system to create a population and/or wave packet, are third-order nonlinear spectroscopies. Depending on the characteristics of input pulses, i.e., their frequencies, polarizations, wave vectors, and time orderings, etc., vastly different systems with different time scales can be studied (and each variation of the measurement technique is likely to have its own name). Most of the techniques utilizing third-order nonlinearity are closely related, although they may look quite different and measure different physical processes. For example, a transient absorption which primarily measures population dynamics of an excited state is closely related to photon echo techniques which are well known to measure an electronic dephasing time. Traditionally, photon echo[40,41] and hole burning[42,43] experiments have been used to remove static components (inhomogeneous broadening) from the absorption spectrum, and thus to obtain dynamical information—the pure dephasing time, T_2. This is possible when the system has two well separated time scales, and its absorption spectrum is dominated by the slower component. Such a time scale separation exists in glasses and crystals at low temperature. For a system with many different time scales and/or for a system where inhomogeneous broadening is not the dominant line broadening mechanism, these techniques can be very difficult if not impossible to interpret unambiguously.[40,41,44–46]

The photon echo technique has been used extensively for the study of dynamics in solids. With the advent of femtosecond lasers, especially Kerr lens mode-locked Ti:sapphire lasers capable of generating ~10 fs pulses,[47] the photon echo

technique has been extended to the study of dynamics in room temperature liquids,[38,44,48–57] where the optical dephasing time[58] is as short as a few tens of femtoseconds. The three pulse stimulated photon echo (3PE) has proven to be very useful in determining the time scales of the system–bath interaction over a wide dynamic range, from a few femtoseconds to several nanoseconds.[38,44] A novel six-wave mixing (fifth-order three pulse echo) technique has been used to reveal the inertial nature of the early (<100 fs) solvation dynamics.[38,45] A gated photon echo technique, where the echo signal for a fixed τ delay is time resolved to determine the ''bare echo'' signal as a function of t' (see Fig. 2), has also been used.[56] Phase-locked photon echoes have also been used to separately measure the real and the imaginary part of a line broadening function, $g(t)$ [see in Eq. (3)].[57,59] It has been recognized for some time that pump/probe transient absorption[33,60] and transient grating[61] measurements can also be used for the study of solvation dynamics. Also, resonance Raman scattering and fitting of absorption spectra can also be used for the study of solvent dynamics.[62]

Most of the experimental data on solvation dynamics with good time-resolution has been obtained using time-resolved fluorescence (TF) utilizing the up-conversion method.[16,28–32,63] A characteristic frequency of the fluorescence spectrum is measured as a function of time, and the Stokes shift function, $S(t)$, is constructed:[64]

$$S(t)=\frac{\nu(t)-\nu(\infty)}{\nu(0)-\nu(\infty)}, \tag{1}$$

where ν's are, for example, the first moment of the fluorescence spectrum at times zero, t, and infinity. In the high temperature limit, $S(t)$ is identical to the transition frequency correlation function:[65]

$$M(t)=\frac{\langle \Delta\omega(0)\Delta\omega(t)\rangle}{\langle \Delta\omega^2\rangle}, \tag{2}$$

where $\Delta\omega(t)=\langle\omega_{eg}\rangle-\omega(t)$. Here $\langle\omega_{eg}\rangle$ is the average transition frequency and $\omega(t)$ is the transition frequency at time t, and the brackets indicate ensemble average. This transition frequency correlation function will be seen to underlie all three techniques considered, thus establishing a very close connection with the fluorescence studies. Typical $S(t)$ functions obtained from fluorescence measurements usually exhibit strongly bimodal character with a fast time constant of 100~200 fs.[16,28–30] Recently, Maroncelli and co-workers presented a comprehensive series of fluorescence measurements of coumarin 153 in various polar and nonpolar solvents.[16] The 100~200 fs process was identified as an inertial response of solvent while diffusive dielectric relaxation processes are responsible for the longer time scales.

In this paper, we present a comprehensive theoretical and experimental study on three different but closely related time domain third-order nonlinear spectroscopies: pump/probe transient absorption (TA), transient grating (TG), and three pulse photon echo peak shift (3PEPS) measurements on a system where the input pulses are resonant (or near-resonant) with an electronic transition. In the theory section (Sec. III) we show in detail how these measurements can give dynamical information of a system, and how each technique is related to others. Third-order nonlinear signals are calculated numerically starting from a single transition frequency correlation function [Eq. (2)], $M(t)$. It is shown through numerical simulations that $M(t)$ can be obtained using the three techniques. In particular, the 3PEPS signal is shown to follow $M(t)$ directly. In the experimental section, we present 3PEPS, TG, and TA measurements for two dyes (HITCI and IR144) in several polar solvents. The results confirm and illustrate the theoretical predictions of Sec. III. They also allow us to obtain $M(t)$ functions for each of the solvent systems and to further dissect $M(t)$ into its contributions from intra and intermolecular dynamics. We briefly compare our results with the fluorescence studies of Ref. 16.

II. EXPERIMENT

The laser system and experimental setup for the three pulse time-resolved measurements has been described previously.[66] A cavity-dumped Kerr lens mode-locked Ti:sapphire laser with a center frequency of 780 nm is used. The laser generates near transform-limited pulses as short as 16 fs with a pulse energy of over 40 nJ at repetition rates up to 1 MHz. The laser spectrum is nearly Gaussian with a bandwidth of ~50 nm (FWHM). Pulse autocorrelation functions measured in a ~30 μm KDP crystal suggest that the temporal profile of the pulse is also close to Gaussian. A pair of external LaKL21 prisms are used to compensate for the group velocity dispersion (GVD) from the optical components. The experimental setup is a general three beam optical delay line setup configured in a ''box'' geometry. The three beams form an equilateral triangle when viewed from the beam propagation direction. Two of the beams are delayed by stepper motor driven translation stages (Klinger) with minimum step sizes of 0.1 and 0.02 μm. For the echo and transient grating measurements the pulses are split into three equal energy pulses and focused by a 10 cm focal length lens. A p-reflection from a BK7 window is used as a probe beam in the transient absorption measurement.

To minimize the thermal grating effect and other higher-order phenomena, pulses are attenuated to ~1.0 nJ (unless specified) before the first beam-splitter and used at a repetition rate of 152 kHz. The samples were circulated at a speed of ~5 cm^3/s through a 100 μm quartz flow cell. At this pulse energy and repetition rate, thermal grating and other high intensity effects are negligible. All of the measurements were performed at room temperature. Infrared dyes HITCI and IR144 are used as received from Exciton Co. The dyes were added to the solutions until the pulse transmittance became ~70%, which results in a dye concentration of $\sim 2\times10^{-4}$ M for IR144 and $\sim 5\times10^{-4}$ M for HITCI.

III. THEORY AND NUMERICAL CALCULATIONS

A. Response functions

All of the nonlinear spectroscopic signals can be conveniently calculated using the response function formalism.

The response functions for the third-order nonlinear spectroscopic techniques have been presented previously by many authors.[67–69] Mukamel and co-workers have presented a comprehensive theory on the nonlinear response function formalism together with the Brownian oscillator model as a bath dynamics.[65,67] In the Brownian oscillator model, each nuclear mode is treated as a harmonic oscillator subject to a Langevin equation with time-independent friction. The formalism presented below can be found in Ref. 67, and is repeated here for completeness. We consider a molecular system with two electronic states, $|e\rangle$ and $|g\rangle$, coupled with external electromagnetic fields through electric dipole interactions. The center transition frequency of the molecular system is ω_{eg}, and the electromagnetic fields are resonant (or near resonant) with the $e-g$ transition. Three different but closely related third order nonlinear time-resolved spectroscopic techniques, i.e., pump/probe transient absorption (TA), transient grating (TG), and three pulse stimulated photon echo (3PE) measurements are investigated.

Dephasing is described by the fluctuations of a transition frequency[70] and thus a key quantity in describing all of the measurements is an electronic Bohr frequency correlation function, $M(t)$. All of the relevant system dynamics are contained in $M(t)$. Using $M(t)$ is equivalent to a spectral density approach used in a previous report.[38] A line broadening function, $g_i(t)$, for a mode i can be calculated from $M_i(t)$:[67]

$$g_i(t)=i\lambda_i\int_0^t dt_1\ M_i(t_1)+\langle\Delta\omega_i^2\rangle\int_0^t dt_1\int_0^{t_1} dt_2\ M_i(t_2), \tag{3}$$

where λ_i is a reorganization energy and $\langle\Delta\omega_i^2\rangle^{1/2}$ is a coupling strength. λ_i and $\langle\Delta\omega_i^2\rangle$ are related by the fluctuation–dissipation theorem. In the high temperature limit ($\hbar\omega_i \ll k_BT$), $\langle\Delta\omega_i^2\rangle=2k_BT\lambda_i/\hbar$ and the solvent Stokes shift is $2\lambda_i$.[65] The high temperature limit is likely to hold in most cases, since the solvent spectra of most liquids are centered around 60 cm^{-1}.[21] For a typical multimode system, $g(t)=\Sigma_i g_i(t)$. The steady-state absorption and emission spectra of the system can be calculated easily from $g(t)$:[65,67]

$$\sigma_A(\omega)=\int_{-\infty}^{\infty} dt\ \exp[-i(\omega-\omega_{eg})t]\exp[-g(t)], \tag{4a}$$

$$\sigma_E(\omega)=\int_{-\infty}^{\infty} dt\ \exp[-i(\omega-\omega_{eg})t]\exp[-g^*(t)], \tag{4b}$$

where ω_{eg} is the center transition frequency of the $e-g$ system and the subscript A and E indicate absorption and emission, respectively. Thus, the real and imaginary parts of $g(t)$ have a simple physical interpretation. The real part of $g(t)$ determines the width of the transition while the imaginary part determines the center transition frequency at time t. When the imaginary part of $g(t)$ is ignored, the absorption and the emission spectra are identical with each other and their widths are determined by the real part of $g(t)$. For a system which can be described by a single $M_i(t)$,$g_i(t)$ is fully determined once $\langle\Delta\omega_i^2\rangle$ (or λ_i) and $M_i(t)$ are known. For a real system where dynamics results from many processes, the real and imaginary parts of each $g_i(t)$ must be added separately to get $g(t)$. In the high temperature limit, where $\langle\Delta\omega_i^2\rangle$ and λ_i have the same linear relation for every mode ($\langle\Delta\omega_i^2\rangle=2k_BT\lambda_i/\hbar$), a single $M(t)$ can still be used to calculate both the real and the imaginary part of $g(t)$. In this case, each mode carries a relative coupling strength in $M(t)[=\Sigma_i\langle\Delta\omega_i^2\rangle_r M_i(t)$, where the subscript r indicates relative coupling strength].

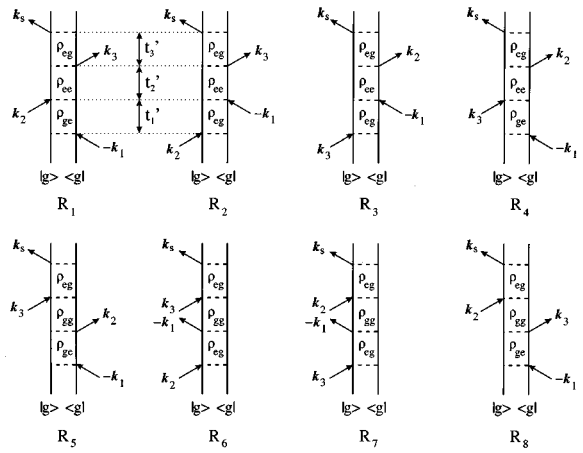

FIG. 1. Two level system (excited, $|e\rangle$, and ground, $|g\rangle$ states) double-sided Feynman diagrams for third-order nonlinear optical spectroscopies in the rotating-wave approximation. The third order polarization has a phase matching direction of $-\mathbf{k}_1+\mathbf{k}_2+\mathbf{k}_3$. The left and right vertical lines represent the ket and bra of the density matrix, respectively. Time increases from bottom to top. **k** represents the wave vector of the in/out-going field. The arrows on the left and right vertical lines represent the field–matter interactions on the ket and bra states, respectively. For a complete description of the Feynman diagram and other diagrammatic techniques, refer to Refs. 67(a), 83, 112, and 113. 1, 2, and 3 are input pulses and S denotes signal polarization. ρ_{ij} represents a nonzero density matrix element during the time interval. After the second field–matter interaction, R_1-R_4 create an excited state population while R_5-R_8 create a ground state population.

For the weak-field limit where the perturbation theory is valid, the third order polarization requires three field–matter interactions at times t_i by electric fields $\mathbf{E}_i(\mathbf{t}_i,\omega_i,\mathbf{k}_i)$, where the subscript i runs from 1 to 3. ω_i and $\mathbf{k}_i$ are the carrier frequency and the wave vector of the pulse i, respectively. The third-order polarizations, $\mathbf{P}^{(3)}(t')$, radiated into the phase-matching directions $\pm\mathbf{k}_1\pm\mathbf{k}_2\pm\mathbf{k}_3$ are created by the three interactions. In the following, we consider a signal radiated into the phase-matching direction $-\mathbf{k}_1+\mathbf{k}_2+\mathbf{k}_3$. This is not a limitation, since we allow all the possible time orderings for the three interactions. For a TA measurement, $\mathbf{E}_1$ and $\mathbf{E}_2$ come from the same pulse, and thus the signal phase matching direction, $-\mathbf{k}_1+\mathbf{k}_1+\mathbf{k}_3$, is equal to the probe beam direction. However, $-\mathbf{k}_1+\mathbf{k}_2+\mathbf{k}_3$ will be used for the TA measurement also, since positive $(+\omega_i)$ and negative $(-\omega_i)$ Fourier components are treated as different frequencies. There are 48 different Liouville space pathways (for degenerate frequencies, there are 24 pathways) to create $\mathbf{P}^{(3)}(t')$ in the $-\mathbf{k}_1+\mathbf{k}_2+\mathbf{k}_3$ direction. When the fields are resonant only with the $e-g$ transition, eight fully resonant Feynman diagrams can be obtained as shown in Fig. 1. In the impulsive limit with fixed time ordering, only two diagrams need to be

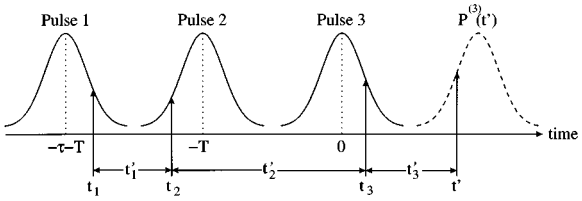

FIG. 2. Time ordering of pulse sequences and notations for various times and time intervals. τ and T denote the center to center distances between the pulse pairs (1, 2) and (2, 3), respectively. t_1, t_2, and t_3 denote field–matter interaction points, while t_1', t_2', and t_3' denote the delays between the interaction points. $P^{(3)}(t')$ is the third order polarization generated by the three interactions at t_1', t_2', and t_3'.

considered for each phase-matched signal. In general, however, it is necessary to keep all of them. The time ordering of the pulses and the notations used for time delays are shown in Fig. 2. t_1, t_2, and t_3 indicate the field–matter interaction points to create the third-order polarization, $P^{(3)}(t')$, at t', while t_1', t_2', and t_3' represent time delays between the interaction points as shown in the figure. The center to center distances of the pulses 1 and 2 and the pulses 2 and 3 are τ and T, respectively. τ and T are the delays that can be controlled in an actual experiment. In the delta function fields limit, $t_1'=\tau, t_2'=T,$ and $t_3'=t'$.

Once $g(t)$ is given, the response functions corresponding to the Feynman diagrams listed in Fig. 1 can be calculated using a second order cumulant expansion:[67]

$$R_1(=R_4)=\exp\{-g^*(t_1')+g(t_2')-g^*(t_3')-g^*(t_1'+t_2') -g(t_2'+t_3')+g^*(t_1'+t_2'+t_3')\}, \tag{5a}$$

$$R_2(=R_3)=\exp\{-g(t_1')-g^*(t_2')-g^*(t_3')+g(t_1'+t_2') +g^*(t_2'+t_3')-g(t_1'+t_2'+t_3')\}, \tag{5b}$$

$$R_5(=R_8)=\exp\{-g^*(t_1')+g^*(t_2')-g(t_3')-g^*(t_1'+t_2') -g^*(t_2'+t_3')+g^*(t_1'+t_2'+t_3')\}, \tag{5c}$$

$$R_6(=R_7)=\exp\{-g(t_1')-g(t_2')-g(t_3')+g(t_1'+t_2') +g(t_2'+t_3')-g(t_1'+t_2'+t_3')\}. \tag{5d}$$

The second-order cumulant expansion is exact when the variable follows Gaussian statistics. The Condon approximation is also used in addition to the approximations used already (electric dipole interaction and the rotating wave approximation). A third-order polarization, $P^{(3)}(t')$, is created via the response functions and it acts as a source term for the various third-order nonlinear signals.

The diagrams shown in Fig. 1 can be divided into two groups: Those that can cause rephasing (R_1, R_4, R_5, R_8) thus form an echo and those that cannot cause rephasing (R_2, R_3, R_6, R_7). For the response functions that can cause rephasing, the polarization during the first coherence period (t_1') and that during the second coherence period (t_3') are complex conjugates of each other, while they have the same sign for those that cannot cause rephasing. The third-order polarization decay, $P^{(3)}(t')$, for the nonrephasing diagrams, is close to a free induction decay (FID). When $t_1'=0$, however, the third-order polarization is always a FID for both the rephasing and the nonrephasing response functions. A trivial yet critical point here is that the rephasing action relies on the correlation between the evolution during t_1' and that during t_3'. As t_2' increases, the system loses memory on the transition frequency, and thus the signal from the rephasing diagrams approaches those of the nonrephasing diagrams. In the long time limit, where $M(t)=0$, the rephasing and nonrephasing terms will contribute equally to the signal—$P^{(3)}(t')$ from both rephasing and nonrephasing diagrams then represent a free induction decay vs t'. The action of rephasing is critical to the third-order signal and thus to the study of the dynamics.

The diagrams shown in Fig. 1 can also be divided into two groups in a different way: Those that create population in the excited state (R_1-R_4) and those that create population in the ground state (R_5-R_8). During the time interval t_2' (this correspond to T in the impulsive limit), the system evolves either in the ground (R_5-R_8) or in the excited state (R_1-R_4) surfaces. Response functions that create excited state population contain an additional decay resulting from the excited state lifetime[71] as well as the decay resulting from $M(t)$. The response functions that create ground state population, however, do not actually create a population grating which is essential in generating the signal—they create a wave packet (hole) in the ground state. Once the ground state dynamics which modulates the transition frequency is over, they no longer contribute to the signal. In the calculations below, we dropped the R_5-R_8 terms, since the wavepacket dynamics from both ground and excited states are included in $M(t)$ (they are indistinguishable in an experiment unless known from an independent source[72]).

B. Model $M(t)$ and the numerical calculation of the response functions

Since $M(t)$ is a transition ($|e\rangle-|g\rangle$) frequency correlation function, fluctuations both in the ground and excited states are important. This is true even in a time-resolved fluorescence measurement where only the excited state wave packet is created.[73] After an instantaneous electronic transition, the system responds to the perturbation (for example, the dipole moment of the solute in the ground and the excited state may differ), and the response of the system modulates the $e-g$ transition frequency. In the case of weak solvent–solute coupling, where the perturbation due to the $e-g$ transition is small, the eigenstates of a solute will resemble those of the isolated molecule. The vibrational levels are generally only weakly coupled with the solvent, i.e., the vibrational energy in an electronic state is only weakly dependent on the solvent–chromophore configuration. If indeed the vibrational levels in an electronic state are only weakly coupled with the chromophore–solvent configuration, the vibrational energy during T is mostly preserved. That is, the electronic transition energy fluctuates rapidly, but the potential energy curve of the chromophore does not undergo significant change.

Therefore the vibrational linewidth is relatively sharp both in the ground and excited state even though the electronic absorption line shape is not, and this is why a hole cannot be burnt for an electronic absorption band even though the chromophore has narrow vibrational transitions. The contributions to $M(t)$ may then be separated into intramolecular wave-packet motions and chromophore–bath dissipation processes (vertical fluctuation of the potential curves). This separation into intramolecular (chromophore) and intermolecular (chromophore–bath) modes will not always be clear cut. The solvent modes generally have a continuous spectrum peaked at relatively low frequencies and lead to apparently irreversible relaxation, whereas the higher frequency intramolecular modes with narrow widths (slow dephasing) produce oscillatory shifts in the transition frequency. However, if the molecule itself contains many strongly coupled low frequency modes it may not be possible to make a distinction between system and bath (i.e., the molecule acts as its own bath).

In principle, the energy levels (and the transition frequency) can be calculated once the solute–solvent configuration is known. For the configuration dependent electronic energies of the ground and the excited states, a simulation by Root is enlightening.[74] It was found that ground and excited states electronic energies are very strongly dependent on the solvent configuration. However, they are strongly correlated with each other, i.e., the transition energy is not as strongly dependent on the solvent–solute configuration as the electronic energy of a state. If the chromophore–solvent configuration is stationary on a time scale of $(\Delta E)^{-1}$, where ΔE is a distribution of the energy that a particular process may span, this distribution directly represents an absorption spectrum. This limit is the so-called *slow modulation limit* (inhomogeneous broadening). A chromophore in a low temperature glass is a typical example. When the configuration is not stationary on a time scale of $(\Delta E)^{-1}$, the distribution no longer represents the absorption spectrum and the fluctuation time scale becomes critical. In the so-called *fast modulation limit*, where the fluctuation is much faster than $(\Delta E)^{-1}$, the line broadening is homogeneous. In liquids there are multiple (even continuous) fluctuation time scales over a broad time range, and classification into homogeneous and inhomogeneous broadening is inappropriate. Here we attempt to represent real liquid systems with a few distinct time scales using a model $M(t)$.

A single dynamical process can also be described at several different levels of sophistication. In the simplest—the optical Bloch limit—dynamics are either infinitely fast (homogeneous) or stationary (inhomogeneous): $M(t)=1$ for inhomogeneous broadening and $M(t)=\delta(t)$ for homogeneous broadening. Also $g(t)$ is real ($\lambda=0$) in the Bloch model—the center transition frequency does not change in time, although $g(t)$ can be extended to a complex form with an appropriate λ using Eq. (3). For the well-known Kubo stochastic model, $M(t)=\Delta^2 \exp(-t/\tau_c)$ and $g(t)$ is given by[68,69]

$$g(t)=(\Delta\tau_c)^2\{\exp(-t/\tau_c)+t/\tau_c-1\}, \tag{6}$$

where Δ is the rms Gaussian fluctuation amplitude. As with the Bloch model, in the Kubo stochastic model the center transition frequency does not change in time-$g(t)$ is real. When $M(t)$ has a finite time scale, the system retains transition frequency information for $t<\tau_c$. For $t\gg\tau_c$, however, the system loses the information on the transition frequency and the rephasing is no longer possible. That is, the dynamics of the system is in its static (inhomogeneous) limit for a small T but it is in the fast modulation limit for $T\gg\tau_c$. This passage from inhomogeneous to homogeneous for a single stochastic process has been discussed previously by Loring and Mukamel.[75] This is the basic principle of how the time-resolved techniques discussed here can be used for the study of dynamics.

In the Brownian oscillator model, $M(t)$ is just a damped harmonic oscillator when the friction kernel in the generalized Langevin equation is approximated as a delta function (time-independent friction).[67] In the Brownian oscillator model, $g_i(t)$ is given by Eq. (3) and thus the imaginary part of $g_i(t)$ is not zero—the center transition frequency is time dependent. The Brownian oscillator model gives physically correct initial behavior where the dynamics must be inertial in contrast to the Kubo stochastic model which has diffusive behavior even at time zero. That is, $[dM_i(t)/dt]_{t=0}=0$ for a Brownian oscillator. For the overdamped Brownian oscillator, the real part of the response function behaves similarly to the Kubo model.

The response functions can be calculated easily once $g(t)$ is known. 3PE and TG signals as a function of t' in the impulsive limit are the modulus squared of the appropriate response functions given by the time ordering. Transient absorption is a heterodyned signal between the third-order polarization and the probe field. Figure 3 shows the rephasing, $|R_1(t')|^2$, and nonrephasing, $|R_2(t')|^2$, response functions vs t' for a slightly over-damped Brownian oscillator. The delay between the first and the second interactions, τ, is set to 30 fs. The population decay is not included. The Brownian oscillator has an $M(t)$, whose time constant, τ_c,[76] is ~100 fs. For small T, the rephasing response function, $|R_1(t')|^2$, peaks near 30 fs revealing an echolike signal although no static inhomogeneous broadening is included in the calculation. That is, at times smaller than τ_c, memory of the transition frequency is retained enabling a rephasing process. For long T, $|R_1(t')|^2$ does not show an echo indicating that the system lost its memory of the transition frequency, and rephasing is no longer possible. Also, note that the area under $|R_1(t')|^2$ decreases as T increases. In the conventional Bloch model, wide inhomogeneous broadening is essential to create an echo. Moreover, the response functions do not depend on T. As shown in Fig. 3(b), the nonrephasing response function, $|R_2(t')|^2$, decays monotonically at all T's. However, it is interesting to note that $|R_2(t')|^2$ actually slows down slightly as T increases, and thus the area under $|R_2(t')|^2$ increases slightly as T increases. Physically, this arises from the fact that $M(t)$ should be a decreasing function for any dissipative physical processes. For our choice of $M(t)$, the real part of $g(t)$ is quadratic around $t=0$, while it is linear in the large t limit. Therefore a sum of the four terms involving t_2' in the exponent of $R_2(t)$ [Eq. (5b)] is

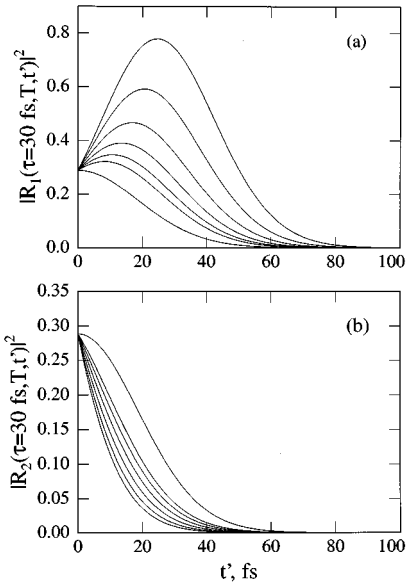

FIG. 3. Modulus squared of the rephasing, $|R_1|^2$, (a), and nonrephasing, $|R_2|^2$, (b) response functions vs t' for a near-critically overdamped Brownian oscillator model $M(t)$. Δ, ω, and γ are 200, 115, and 240 cm^{-1}, respectively. τ is set to 30 fs, while T is varied: (a) from top to bottom, $T=0$, 20, 40, 60, 80, 100, ∞ fs; (b) from bottom to top, $T=0$, 20, 40, 60, 80, 100, ∞ fs. Note that $|R_1|^2$ and $|R_2|^2$ are identical at $T=\infty$.

always negative with an asymptotic value of zero. Thus, the area under $|R_2(t')|^2$ always increases as T increases. These facts are critical in understanding how the solvation process is manifested in the time-resolved third-order nonlinear spectroscopies discussed below.

C. Three pulse photon echo peak shift (3PEPS)

In the three pulse stimulated photon echo (3PE) measurement, the signal (integrated over t') into the phase-matching direction of $-\mathbf{k}_1+\mathbf{k}_2+\mathbf{k}_3$ is measured as a function of τ for a fixed T. In the impulsive limit where the pulse duration is much shorter than any of the dynamical time scales of the system, the signal is proportional to the modulus squared of the response function:

$$I(\tau,T)\propto\int_0^\infty dt'|R(\tau,T,t')|^2. \tag{7}$$

The echo signal in the impulsive limit can be understood easily.[44,67(c)] The pulse sequence for $\tau>0$ is 1–2–3, while it is 2–1–3 for $\tau<0$. For τ positive, the rephasing diagram R_1 is the only nonzero term, while the nonrephasing diagram R_2 is the only nonzero term for $\tau<0$. Thus the 3PE signal for $\tau>0$ and $\tau<0$ represents the integrated (over t') rephasing and non-rephasing response functions, respectively. Figure 4 shows 3PE signals for several different T values for the same Brownian oscillator form for $M(t)$ as used in Fig. 3. For T smaller than the time constant of $M(t)$, the signal shows asymmetry indicating that the system's rephasing ability. For $T\gg\tau_c$, the system can no longer rephase and the signal becomes symmetric. It is interesting to note that the 3PE signal vs τ shows a maximum at positive τ even in the impulsive

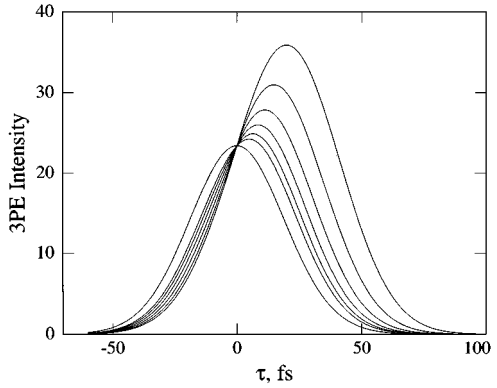

FIG. 4. Three pulse stimulated photon echo signal (integrated over t') vs τ for several values of T, the population period, in the impulsive limit calculated using the same Brownian oscillator $M(t)$ as in Fig. 3. From top to bottom, $T=0$, 20, 40, 60, 80, 100, ∞ fs.

limit. This is in contrast to the common notion that the echo signal should decay monotonically as τ increases, and that the echo signal may peak at positive τ only through the finite pulse duration—the effect of convolution. This peak shift from $\tau=0$ in 3PE is due to the fact that the measured signal is an integration over t'. Figure 5 shows the $|R_1|^2$ as a function of t' for several τ values. When τ is zero, full rephasing occurs at $t'=0$ and thus the signal decreases monotonically as t' increases. However, when τ is not equal to zero but less than the irreversible decay time scale, the peak of the 3PE signal vs t' appears at $t'=\tau$ due to the rephasing process, and thus the area over t' increases. Further increase of τ causes a decrease in the signal as a result of irreversible dephasing. Thus the 3PE signal vs τ shows a characteristic shift from $\tau=0$. Since this shift is related to the rephasing capability, it becomes smaller (the signal becomes more symmetric w.r.t.

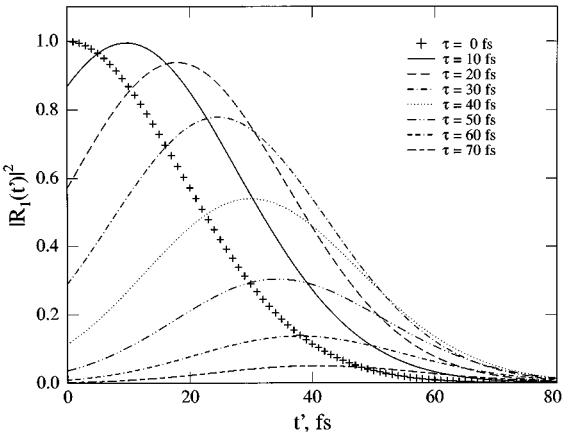

FIG. 5. Demonstration of the shift to positive τ values in a three pulse echo signal (3PE vs τ). The rephasing response function, $|R_1|^2$, is plotted vs t' for different τ values using the same Brownian oscillator used in Fig. 3. For small τ values, the curve is peaked at $t'=\tau$ as a result of rephasing. Note that the area under each curve (i.e. the echo signal integrated over t') initially increases with increasing τ as a result rephasing of even though the maximum value of the rephasing function decreases.

τ) as T increases, and the rephasing capability diminishes. When the peak shift is measured as a function of T, the shift is found to follow $M(t)$ closely. Recently, Cho *et al.*[77] have shown that the time dependence of the peak shift is very close to $M(t)$ for $t \geqslant 100$ fs. It is not difficult to see that the 3PE peak shift should occur even in the Bloch limit when the homogeneous and inhomogeneous widths are comparable.[44] In the Bloch limit, however, the shift is small and does not change as T changes.

In a typical photon echo measurement in a room temperature liquid, the pulse duration is comparable to the dephasing time scale and the pulse field envelope must be convoluted with the response functions with proper time orderings. In actual 3PE measurements, it is important to keep the population period (the delay between the second and the third pulse) constant for both positive and negative τ during a scan. In the 3PE measurement performed here, two phase-matched signals at $\mathbf{k}_1-\mathbf{k}_2+\mathbf{k}_3$ and $-\mathbf{k}_1+\mathbf{k}_2+\mathbf{k}_3$, which are mirror images to each other, are measured simultaneously.[44,49] To keep T constant, especially for small T, the scan is done as follows. Initially, pulse 1 is being scanned while pulse 2 and 3 are stationary. In this case pulse 1 arrives at the sample first ($\tau>0$), and pulse 2 and 3 are separated by T. When pulse 1 reaches $\tau=0$, i.e., overlaps with pulse 2, pulse 3 starts to move in parallel with pulse 1. That is, for $\tau<0$, the pulse sequence is 2–1–3 with pulse 2–1 and 1–3 separations of $|\tau|$ and T, respectively. The third-order nonlinear polarization for a given t, T, and t' is now a sum of all four possible time orderings (R_1 through R_4), and each term is represented by the convolution of the response function with the field envelopes with proper time ordering:

$$P^{(3)}(\tau,T,t') \propto \int_0^\infty dt_3' \int_0^\infty dt_2' \int_0^\infty dt_1' \sum_{i=1}^{4} R_i(t_1',t_2',t_3') \times \mathbf{E}_1^*(\mathbf{k}_1,t_1)\mathbf{E}_2(\mathbf{k}_2,t_2)\mathbf{E}_3(\mathbf{k}_3,t_3), \tag{8}$$

where $\mathbf{E}_i$ is an electric field with a wave vector $\mathbf{k}_i$. In the actual experiment, the 3PE signal, $|P^{(3)}(\tau,T,t')|^2$, integrated over t' is measured as a function of τ and T.

The effect of finite pulse duration is shown in Fig. 6 where the peak shift in 3PE is calculated for a Gaussian field envelope. In all of the calculations (3PEPS, TG, and TA) including field envelopes, the pulses are always transform limited. That is, once the pulse duration is determined, the frequency spectrum is determined automatically. Also the excited state lifetime is set to infinity—the signal decay is solely due to the solvation dynamics excluding population relaxation. As expected, the peak shift increases as the pulse duration increases. Nevertheless, the time constants obtained from moderately long pulses are remarkably similar to the time constant in the impulsive limit. This feature will be extremely useful for the measurements of ultrafast processes such as the initial solvation of a solute in water which is calculated to be ~50 fs for large molecular solutes,[18,21(b),22,23,26,78,79] but has not yet been completely time resolved.[30] The insensitivity to pulse duration will also be useful when the pulse frequency spectrum must be narrow to achieve spectral selectivity.

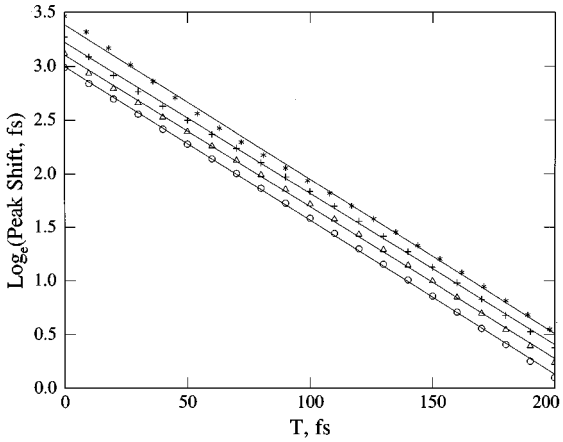

FIG. 6. The effect of pulse duration on the three pulse echo peak shift (3PEPS) as a function of the population period, T, is shown for the same Brownian oscillator used in Fig. 3. The pulse durations (FWHM of the pulse intensity profile) are; *, 40 fs; +, 20 fs; Δ, 10 fs; ○, 0 fs. The time constants obtained from a linear fit (solid lines) are from top to bottom, 69.7, 70.7, 71.0, and 69.5 fs, respectively.

The insensitivity of the 3PEPS to the pulse duration can also be illustrated in a different way. Figure 7 shows calculated 3PE signal at $T=0$ (a) and 3PEPS (b) signals for various pulse durations. $M(t)$ now contains an oscillatory component (a damped cosinusoid) to mimic an intramolecular

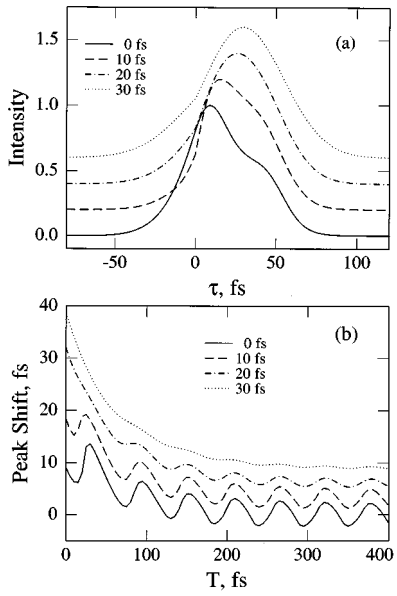

FIG. 7. The effect of pulse duration on (a) individual normalized 3PE signals and (b) 3PEPS are shown for a system with a fast oscillation in $M(t)$. The curves are offset by 0.2 in (a) and by 3 fs in (b), successively. The $M(t)$ is a sum of the Brownian oscillator used in Fig. 3 and a damped cosinusoid with a frequency of 600 cm^{-1}, damping time of 1 ps, and a coupling strength of 150 cm^{-1}. $T=0$ fs in (a). With a pulse duration of 20 fs, the oscillation is not visible in the 3PE signal (a), although a trace of oscillation is still visible in the 3PEPS signal (b) for a 30 fs long pulse. Also note that the peak shift can be negative in 3PEPS, just as $M(t)$ can.

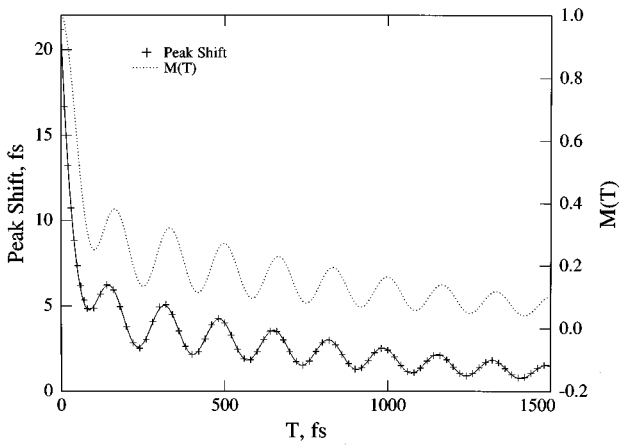

FIG. 8. Model calculation of 3PEPS vs T using an $M(t)$ which composed of an ultrafast Gaussian, an exponential with a time constant 1 ps, and a damped cosinusoid. The pulse is on resonance ($\Delta\omega$ of 0 cm^{-1}) and has a duration of 20 fs. A nonlinear least-squares fit (solid line) of the calculated peak shift using the same functional form as $M(t)$ is also shown. The functional form of $M(t)$ and the parameter values actually used for calculation as well as the fit results are listed in Table I. See the footnote of Table I for details.

mode, in addition to the slightly overdamped Brownian oscillator. For pulse durations much shorter than the period of the oscillation (50 fs) the 3PE signal at $T=0$ (and two pulse echo signal also) clearly shows a shoulder resulting from the oscillatory component. As the pulse duration gets longer, the shoulder is quickly washed out by convolution. In 3PEPS, however, the oscillation is clearly evident with much longer pulses as shown in Fig. 7(b).

To show that 3PEPS actually follows $M(t)$ closely, calculations using model $M(t)$'s were performed, and the calculated 3PEPS are fitted to the functional form of the model $M(t)$. The Model $M(t)$ used is a sum of a Gaussian, an exponential, and a damped cosinusoid. A typical calculated 3PEPS and the fit is shown in Fig. 8 together with the $M(t)$. The fitting results are listed in Table I. The table shows that 3PEPS indeed follows $M(t)$ closely. In particular, the 3PEPS decay times closely match those in $M(t)$ except for the Gaussian component. The actual time constant of the Gaussian in $M(t)$, however, is 56 fs[76] (not 70 fs) and is reasonably close to the time constant from the fit. The phase of the oscillation, however, is shifted significantly ($\sim$20 fs). The amount of the shift, however, does not depend on the frequency or phase in $M(t)$. That is, for a calculation with several oscillatory components, each oscillation will be shifted by the same amount in time units, not in radians. This shift depends weakly on the pulse duration, and increases slightly as the pulse duration increases.

It is interesting to note that the peak shift can also be negative. When the slow exponential component is dropped from the $M(t)$ used above (Fig. 8), the 3PEPS shows an oscillation around zero peak shift. When oscillations in $M(t)$ make the peak shift negative, rephasing occurs at negative τ. For a system with a static component, $M(t)$ will have an offset proportional to the relative coupling strength of the static component. The 3PEPS in this case will also have an offset just as in $M(t)$. This feature will be very useful for detection of static components (inhomogeneity).

D. Transient grating

The transient grating (TG) measurement is very similar to the 3PE measurement. A signal in the same phase-matching direction, $-\mathbf{k}_1+\mathbf{k}_2+\mathbf{k}_3$, is measured while scanning T but now $\tau=0$ (pulse 1 and 2 overlap in time). The measured TG signal is again the time-integrated modulus squared of the third-order polarization:

$$I_{\mathrm{TG}}(T)=\int_{-\infty}^{\infty} dt' |P^{(3)}(0,T,t')|^2. \tag{9}$$

Physically, a spatial transmission grating is formed in the sample by the interference of the two input pulses.[61] The grating is destroyed by processes such as population relaxation, spectral diffusion, and spatial diffusion. A third pulse is scattered off the grating into the Bragg angle. As shown in the previous section, the rephasing process causes the signal to peak at finite τ values. It can be seen easily that in the impulsive limit t_1' is always zero, and the TG is not sensitive to the rephasing process or to a change in the center absorption frequency. For a finite pulse duration t_1' can be as large as the pulse envelope, and rephasing diagrams with nonzero t_1' will contribute to the signal. Thus spectral diffusion (solvation) will only appear in a finite pulse duration measurement when the pulse duration is longer than the electronic dephasing time scale. The imaginary part of the response function also contributes to the signal in the finite pulse du-

TABLE I. Nonlinear least fit results for the calculated 3PEPS, TG, and TA signals using a model $M(t)$.

	A_1	τ_1, fs	A_2	τ_2, fs	A_3	τ_3, fs	ω_3, cm^{-1}	p_3, rad
$M(t)$[a]	0.55	70	0.31	1000	0.14	1000	200	0
3PEPS[b]	0.68[c]	36	0.24	980	0.08	1030	199.2	0.634
TG[d]	0.85	29	0.11	820	0.04	754	198.9	0.30
TA[d]	0.54	54	0.38	1660	0.08	1490	200.6	−0.1

[a]$M(t)$ is specified by $M(t)=A_1\exp(-(t/\tau_1)^2)+A_2\exp(-t/\tau_2)+A_3\exp(-t/\tau_3)\cos(\omega_3 t+p_3)$.
[b]The fitting function is a sum of two exponentials and a damped cosinusoid.
[c]This corresponds to a peak shift of 14.4 fs.
[d]The fitting function is the same as in 3PEPS but convoluted with a Gaussian pulse autocorrelation envelope. Also a base line is added. Time zero and the width of the Gaussian are varied in the fit. When they are fixed to zero and 28.3 fs (the autocorrelation width of the 20 fs pulse used in the calculation), respectively, the fit becomes unacceptable.

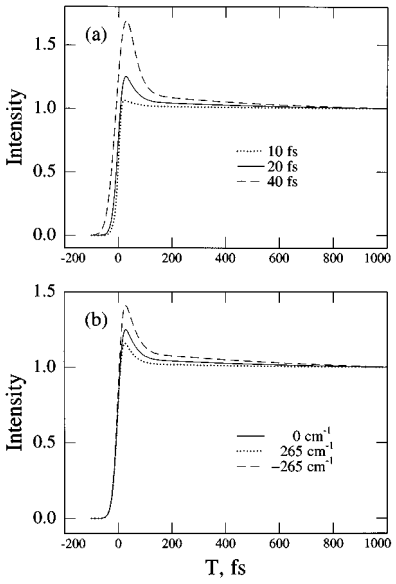

FIG. 9. Model calculation of transient grating (TG) signals based an $M(t)$, which is the same as that used for Fig. 8 except here the damped cosinusoid is dropped for clarity. Thus, there are two time scales in $M(t)$: $A\sim 56$ fs component which gives rise to a spike around $T=30$ fs and a 1 ps component which produces a slow decay. The signals are normalized at $T=1000$ fs. (a) Pulse duration dependence while the detuning ($\Delta\omega$) is fixed at 0 cm^{-1}; (b) Detuning dependence of TG signal with a fixed pulse duration of 20 fs. $\Delta\omega$ is positive when the frequency of the pulse is smaller than the resonance frequency.

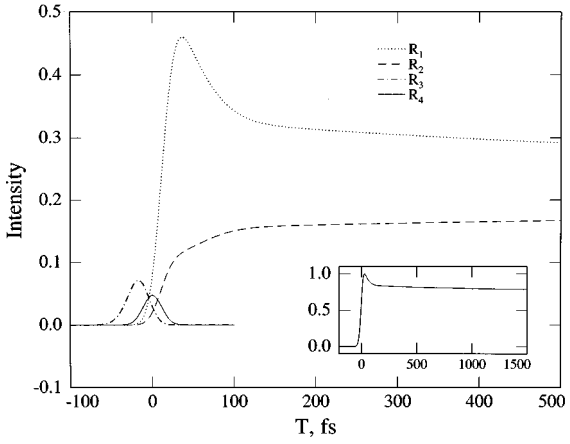

FIG. 10. Calculated TG signal with the same $M(t)$ used in Fig. 9. $\Delta\omega=0$ cm^{-1} and the pulse duration=20 fs. The signal from each response function is shown separately. Inset shows the total TG signal. Note that the R_2 contribution is a rise, and that the R_4 signal is peaked at $T=0$ fs.

ration measurement in contrast to the impulsive limit where the imaginary part of the response function does not contribute to the signal. The imaginary part of $g(t)$ changes the center transition frequency, thus the grating diffraction efficiency will be modulated. Depending on the pulse durations of the pump (pulse 1 and 2) and probe pulses, the signal will have different sensitivities to the real and imaginary parts of $g(t)$. When the pump pulses are longer than the dephasing time but the probe is a delta function, the signal will only be sensitive to the real part of $g(t)$ within the Condon approximation. For delta function pump pulses and long probe pulses, the sensitivity to the dynamics in TG signal comes only from the imaginary part of the response function. For the parameters used here, the imaginary part of $g(t)$ makes a minor contribution to the signal.

In Fig. 9(a), TG signals are calculated for several different pulse durations. Also shown in Fig. 9(b) is the dependence on detuning from exact resonance with the optical transition. The $M(t)$ used in these calculations has an ultrafast Gaussian (70 fs) component and an exponential component with a time constant of 1 ps. Here also the excited state lifetime contribution is neglected. The calculated TG signal can be decomposed into a portion that reflects dynamics and a portion that reflects population (here a constant background). The TG signal clearly shows a decay with similar time constants to those in $M(t)$. As expected, the signal is more sensitive to the dynamics as the pulse duration becomes longer. Also as the input pulses are red-shifted from the center transition frequency ($+265$ cm^{-1}), the TG signal shows less sensitivity to the dynamics. This is due to the fact that the grating efficiency is increased as a result of the dynamic Stokes shift. The imaginary part of $g(t)$ causes the absorption spectrum at t to shift to the red and this results in the probe pulse having a better overlap with the transient absorption spectrum at time t. This partially cancels out the decrease of the signal due to the loss of rephasing capability. In the opposite case, where the input pulses are on the blue side of the transition, both the rephasing and grating efficiency decrease making TG more sensitive to the dynamics.

In TG (and also in TA), there is a spike near time zero (peaked at $\sim$29 fs in Fig. 9), the so-called *coherent artifact.* The spike exists even when only the rephasing (properly time-ordered) diagrams are considered. This spike is a result of ultrafast dynamics in solution (here the Gaussian component) and not purely a result of the nonproperly time ordered diagrams as suggested previously.[80,81(a)] That is, the ultrafast decrease of the TG signal is due to the ultrafast decay in $M(t)$ and the concomitant ultrafast decrease in the rephasing capability. Figure 10 shows the contributions of each response function separately. The nonproperly time ordered diagrams (R_3,R_4) do make small contributions and are peaked around zero delay. It is interesting to note, however, that R_3 (nonrephasing) is peaked at negative delay, while R_4 is peaked at $T=0$. R_1 and R_2 have proper time orderings and they contribute for T outside the pulse overlap region. R_2 increases as T increases, as shown in Fig. 3(b). The asymptotic value of R_1 and R_2 is the same, since in the long T limit $P^{(3)}(t')$ is always a free induction decay. The sensitivity of R_1, however, is larger than that of R_2 and generates the decay in the TG signal.

To show the versatility of the TG measurement a series of model calculations were performed and the calculated results fitted to the functional form of $M(t)$ convoluted with a Gaussian. In all cases, the TG signal follows $M(t)$ closely. A typical example is shown in Fig. 11. The model $M(t)$ used is the same as for 3PEPS. The nonlinear least-square-fit results

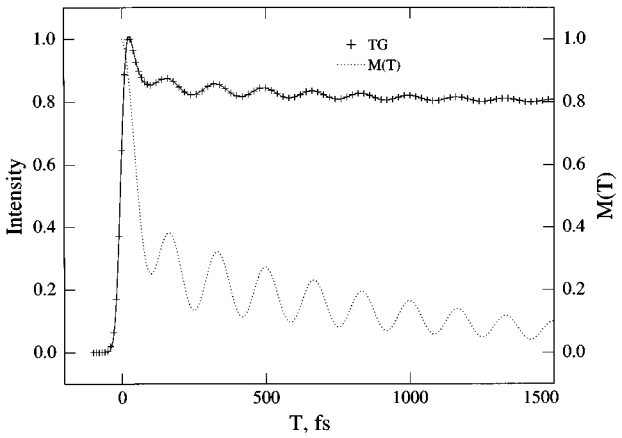

FIG. 11. Comparison of TG signal and $M(t)$. Aside from an offset, the TG signal follows $M(t)$. The $M(t)$ and other parameters used are the same as in Fig. 8. The solid line is a nonlinear least square fit to the calculated TG signal. The fit function and results are listed in Table I.

for the TG case are also listed in Table I. Note that time zero and the width of the Gaussian used in the convolution are varied in the fit. When fixed, the fit becomes unacceptable near time zero. The table shows that the calculated TG signal follows $M(t)$ closely. As in 3PEPS, the oscillations are shifted (see Table I) although the shift is smaller in TG. The TG, however, has an intrinsic background unlike 3PEPS. The offset can be a serious limitation of the TG measurement, since this intrinsic offset cannot be differentiated from the static (inhomogeneous) component in $M(t)$. That is, when the system has a static (on the time scale of the measurement) component, there is an offset in 3PEPS whose magnitude is proportional to the relative coupling strength of the static component. The static component also appears as an offset in TG, but the intrinsic offset in TG will make a static component in $M(t)$ undetectable. It is also harder in TG to get information near time zero than in 3PEPS due to the *coherence spike*, which arises almost entirely from the ultrafast Gaussian component in $M(t)$, at least in this calculation. Also note that the frequency of the oscillation is the same as that in $M(t)$, not doubled, although modulus squared of the polarization is detected in the TG experiment.

E. Transient absorption

In a transient absorption (TA) measurement, $\mathbf{k}_1$ and $\mathbf{k}_2$ come from the same pulse, therefore they overlap in time and have the same carrier frequency. The third-order polarization has a phase-matching direction of $-\mathbf{k}_1+\mathbf{k}_1+\mathbf{k}_3$ $(=\mathbf{k}_3)$. The pulse sequence corresponds to the 3PE measurement while varying T with $\tau=0$ (i.e., the same as in TG). In TA, the third-order polarization is created by the two interactions of the pump pulse and one interaction of the probe pulse. Thus, the third order polarization in TA is identical to that in TG, and all of the signal characteristics in TG should also appear in the TA measurement. In TA, however, the third-order polarization is heterodyned against the probe pulse and this makes the measurement very different from TG. In a typical transient absorption measurement, the probe difference intensity with and without the pump pulse is measured as a function of T, the delay between the pump and the probe.[82,83]

$$I(T)\propto \int_{-\infty}^{\infty} dt'\{|E_{\rm pr}(t')+E^{(3)}(t')|^2-|E_{\rm pr}|^2\}$$

$$=2\ \mathrm{Im}\ \omega_{\rm pr}\int_{-\infty}^{\infty} dt'\ E_{\rm pr}(t')P^{(3)*}(0,T,t'), \tag{10}$$

where $\omega_{\rm pr}$ and $E_{\rm pr}$ are the carrier frequency and field envelope of the probe pulse, respectively. $E^{(3)}(t')$ is the electric field created from the third order polarization $P^{(3)}(t')$. Thus the measurement time window (t') in TA is determined by the probe pulse duration. The time window restriction plays an important role on the sensitivity of the TA signal to the solvation dynamics. By limiting the measurement time window, the rephasing of the third-order polarization which appears for t' away from zero may not be fully detected. Nevertheless the effect of the pulse duration and detuning have the same trend as in TG, as is expected, since the time orderings are the same in the TA and TG measurements. When the pump pulse is long, causing the rephasing term to be dominant, and the probe pulse is also long, the TA signal is sensitive to solvation and spectral diffusion processes. However, unlike the TG signal, when the probe pulse is short, the TA signal is not sensitive to solvation, since the detection time window is determined by the probe pulse duration. For example in a TA signal calculation with the same

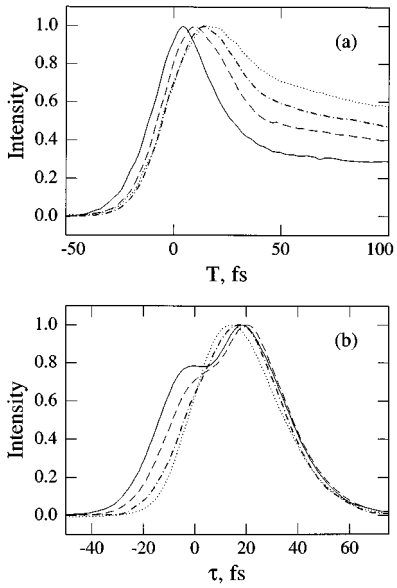

FIG. 12. Measured effects of high pulse intensity on the TG and two pulse echo signals. Peak intensities are estimated assuming a 50 μ diameter beam size and 20 fs long rectangular pulse shape. Intensities are given in W/cm^2 for each beam. (a) TG signal of IR144 in butanol: solid line, intensity$=7.3\times10^9$; dashed line, 3.7×10^9; dash–dotted line, 1.9×10^9; dotted line, 7.5×10^8. Further decrease of the intensity does not change the TG signal. (b) 2PE signal of HITCI in methanol in the $-\mathbf{k}_1+2\mathbf{k}_2$ phase-matching direction: solid line, intensity$=8.1\times10^9$; dashed line, 6.9×10^9; dash–dotted line, 3.4×10^9; dotted line, 4.7×10^8 W/cm^2.

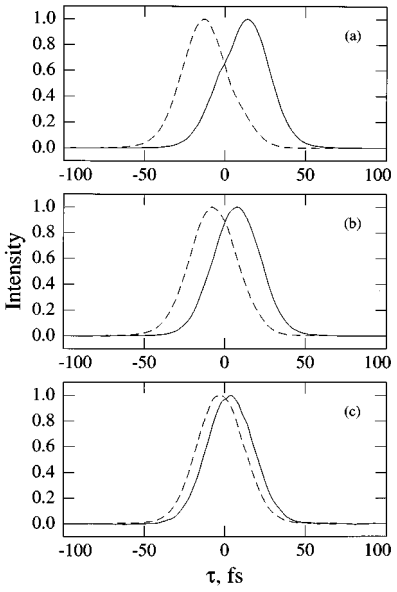

FIG. 13. 3PE signals for IR144 in methanol in two different phase matching directions, $-\mathbf{k}_1+\mathbf{k}_2+\mathbf{k}_3$ (solid line) and $\mathbf{k}_1-\mathbf{k}_2+\mathbf{k}_3$ (dashed line); (a) $T=0$ fs, (b) $T=40$ fs, and (c) $T=1.3$ ps.

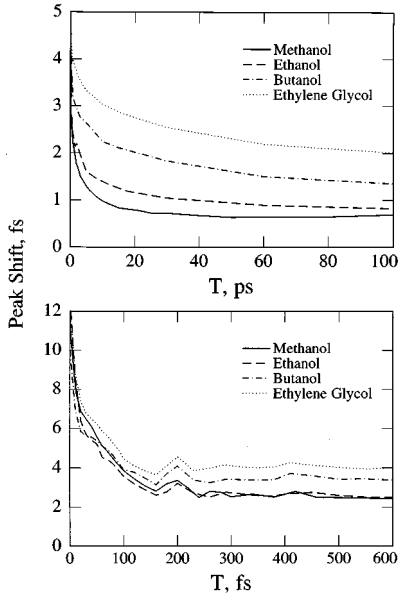

FIG. 14. 3PEPS vs T for IR144 in several solvents: solid line, methanol; dashed line, ethanol; dash–dotted line, butanol; dotted line, ethylene glycol. Note the different time ranges in the top and bottom figures.

$M(t)$ and parameters as in Fig. 9, the TA signal (not shown) does not show any dynamics for a 10 fs pulse, and the TA signal is actually a rise rather than a decay. This is because the heterodyning picks up only the initial part of the third-order polarization (vs t') where the signal is independent of T. The TA signal will also be more sensitive to detuning, since the third-order polarization is heterodyned against the probe pulse. For a detuning of 265 cm^{-1}, the TA signal is a slight rise not a decay, and the dynamics can not be extracted or give a very different time constant than the one fed in to the calculation.

The contribution from each response function is similar to that in TG, except in TA the rise of R_2 almost cancels out the decay in R_1, making the TA measurement less sensitive to the dynamics. Also both R_3 and R_4, the nonproperly time ordered terms, are shifted to positive delays so that now R_3 is centered at zero while R_4 is centered at positive delay. Several TA calculations were carried out and compared with $M(t)$. A TA signal was calculated with the same model $M(t)$ used in 3PEPS (Fig. 8) and TG (Fig. 11), and the fit results are listed in Table I. It is to be noted that the time zero and the width of the Gaussian used in the convolution are also varied in the fit as in TG. When they are fixed, the fit becomes unacceptable near time zero. Unlike 3PEPS and TG, however, the time constants do not match quantitatively with those in $M(t)$. Of course when the dynamical part of the signal is significant, $M(t)$ can be obtained from the calculated TA signal as well.

The TA signal has been calculated previously using the optical Bloch model[80,81(a),84–86] except for studies by Cong *et al.*[81(b)] and Bosma *et al.*[87] where the Brownian oscillator model (and the Kubo model) were used. It is easy to see in the optical Bloch model that the coherence spike must come from the nonproperly time ordered response functions as shown previously.[80,81(a),84–86] Cong *et al.*,[81(b)] however, suggested that part of the coherence spike originates from the rapid solvent fluctuations (solvation dynamics), and our analysis is in agreement with their comments.

IV. EXPERIMENTAL RESULTS

A. Intensity dependence

All of the TA, TG, and photon echo signals show intensity dependence. The effect of high intensity shows up near the pulse overlap region. The intensity effect can significantly modify the initial ultrafast decay of the signal in TA and TG (especially the amplitudes) and needs to be discussed before presenting the main results. In addition for photon echo measurements, the shape of the signal changes with intensity and thus the peak shift is not well determined in the high intensity region. Figure 12 shows the TG signal for IR144 in methanol and two-pulse photon echo signals for HITCI in methanol at various peak intensities. The intensity dependence for both dyes is qualitatively similar, but the threshold for observing the intensity dependent effect is about four times higher in IR144 than in HITCI. Even for the highest pulse energy available from the laser, the two pulse echo (2PE) signal of IR144 does not develop a full double maximum as in HITCI, and only a shoulder appears. As the intensity increases, the initial coherence spike becomes more prominent in the TG signal. The TA signal also shows a qualitatively similar power dependence to the TG signal. In 2PE the top of the signal flattens at lower intensities and develops double maxima at higher intensities. The intensity dependence is not related to a thermal grating, since the signal does not depend on either the repetition rate of the pulses or the flow rate of the sample. The thermal grating is appar-

TABLE II. Three Pulse Echo peak shift and transient grating data for IR144 and HITCI in several solvents. (a) Triple exponential fits plus a baseline to 3PEPS data (fits exclude ~6 fs component arising from intramolecular modes). (b) Three exponential fits to transient grating data.

(a)

	A_1,fs[a]	τ_1,fs[a]	A_2,fs	τ_2,ps	A_3,fs	τ_3,ps
HITCI in glycerol. H_2O	4.85	40.5	1.16	1.8	3.63	83
HITCI in ethylene glycol	5.0	42.5	1.77	2.6	3.69	99
IR144 in ethylene glycol	4.86	49.9	0.98	3.4	1.32	48
IR144 in methanol	5.26	65.0	1.31	1.4	0.91	11
IR144 in ethanol	4.94	61.2	1.19	3.05	0.77	27
IR144 in butanol	3.82	58.5	1.06	3.5	1.13	33

(b)

	A_2	τ_2, ps	A_3	τ_3, ps	A_4	τ_4, ps
IR144 in Methanol[b]	1(1)	1.3(0.9)	0.61(3.1)	9.9(10)	1.32(8.3)	127
IR144 in Ethanol	1	2.4	0.97	25	1.67	191
IR144 in Propanol	1	3.1	1.24	34	1.82	203
IR144 in Butanol	1	3.2	1.1	36	2.14	195
Cresyl Violet in ethylene glycol		3.8				
LD690 in ethylene glycol		3.8				

[a]Note that for A_1 and τ_1, the simulation results in Table I show that A_1 is overestimated and τ_1 underestimated in comparison to their actual values in $M(t)$.
[b]The numbers in parentheses are from TA measurements in methanol with τ_3 and τ_4 fixed at 10 ps and ∞, respectively.

ent only when the cw mode-locked output (78 MHz train) is used directly on a sample in a flow cell rather than a free jet. Also the intensity dependence is not the effect of high dye concentration (dense media effect). Two samples with dye concentrations different by an order of magnitude give identical results. Interestingly, the intensity dependence is correlated with the saturation of the dye. That is, the intensity dependence appears when the dye becomes significantly saturated, i.e., when the change in transmission is no longer proportional to the pump intensity. It is also interesting to note that the saturation pulse intensity of HITCI is also ~four times lower than that of IR144.

A similar intensity dependence in photon echo signals has been reported previously. Leo *et al.*[88] reported 2PE in semiconductors, in which a similar power dependence was observed. At high intensity, the 2PE signal develops a double maximum but the second peak appears at negative delay in contrast to our data where an additional peak appears near time zero. Leo *et al.* attributed the intensity dependence to the result of polarization interactions between excitons. van Burgel *et al.*[89] also reported a similar intensity dependence of 2PE signals of *J*-aggregates in water. They attributed the intensity dependence to excited state (higher exciton bands) absorption. The threshold intensity levels for observing the intensity dependence in both studies were much lower than that in the present study.

We believe the intensity dependence in our signals arises from the interference of the third-order signal with higher-order polarizations. The signals being observed are third-order polarizations. However, there are always signals from fifth-order polarizations radiating into the same phase-matching direction. For example, the 2PE signals in $-\mathbf{k}_1+2\mathbf{k}_2$ phase matching direction always have fifth-order scattering with the same phase-matching direction, for example $-\mathbf{k}_1+(\mathbf{k}_1-\mathbf{k}_1)+2\mathbf{k}_2$, etc. Judging from the strength of the pure fifth-order signal appearing at $+\mathbf{k}_1-2\mathbf{k}_2+2\mathbf{k}_3$, the

TABLE III. Linear prediction-singular value decomposition results for the TG signal from IR144 in ethanol.

Amplitude (A_i)	Frequency (ω_i), cm^{-1}	T_2, fs	Phase (ϕ_i), radian
0.0084	709	1800	−0.09
0.0073	645	1600	1.09
0.037	571	580	1.61
0.17	479	260	−1.18
0.067	437	1000	−0.11
1	317	110	−0.56
0.085	302	890	−0.26
0.053	204	500	0.50
0.35	138	320	0.14
0.062	85	630	0.13

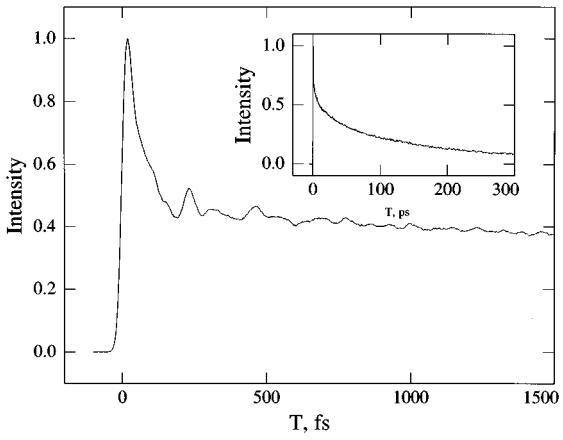

FIG. 15. TG signal of IR144 in methanol. Inset shows data out to 300 ps.

amplitude of the fifth-order polarization may be comparable to the third-order polarization at the highest intensity shown in Fig. 12. Similar interference between third- and fifth-order polarizations has been reported previously.[90] Detailed analysis of this higher-order interference is beyond the scope of this paper and will not be pursued further. However, it is critical to keep the intensity of the input beams low enough to be free from the artifacts due to high intensity phenomena. The pulse energies found to have negligible effect on the signals are 200 and 50 pJ for IR144 and HITCI, respectively, when a 10 cm focal length (singlet) lens is used (it gives ~80% transmission through a 50 μm diameter pin hole).

B. Three pulse photon echo peak shift

3PE signals from IR144 for several different polar solvents were measured using 18~20 fs transform-limited Gaussian pulses. Figure 13 shows typical 3PE signals for IR144 in methanol in the two phase-matching directions $\mathbf{k}_1-\mathbf{k}_2+\mathbf{k}_3$ and $-\mathbf{k}_1+\mathbf{k}_2+\mathbf{k}_3$ for several different T values. Each signal is almost symmetric and has its the peak shifted from $\tau=0$. Each signal is fitted to a Gaussian and the peak shift is defined as half of the peak to peak distance between the two Gaussians. In this way the peak shift is reproducible within ± 0.3 fs. As shown in the previous sections, the peak shift in the 3PE signal (for a fixed T) is a measure of the difference between the echo signals of the rephasing side ($\tau>0$) and that of the nonrephasing side ($\tau<0$). Thus the peak shift in 3PE at a particular T value is a measure of the system's ability to rephase (to cause an echo) after spending time T in a population state, and the 3PE peak shift vs T is a indirect measure of $M(t)$.

Figure 14 shows the peak shift vs. T for several different solvents. All of the data have common features. The 3PEPS decays with several well-separated time scales: The peak shifts decays from ~12 fs at $T=0$ to ~8 fs in ~20 fs, and to ~3 fs within 200 fs. After that 3PEPS decays slowly on two time scales; a few ps and a few tens of ps. For very large T, the peak shift becomes near zero, indicating that there is no static inhomogeneity in a room temperature liquid. It is interesting to see that the 3PE peak shift for different solvents are almost identical for T up to ~500 fs. However, they are clearly different in the long time scales as can be seen in the top part of Fig. 14. The 3PEPS data excluding the portion $T<20$ fs are fitted to three exponentials and the results listed in Table II. It can be seen that the ultrafast time scale (τ_1) is the same from methanol to ethylene glycol although their viscosities are vastly different. The amplitudes of the ultrafast components are, however, solvent dependent. All of the 3PEPS curves have identical oscillations, which originate from intramolecular vibrations of IR144. The same oscillations are also found in the TG and TA measurements (vide infra).

Even though the initial drop (from ~12 to ~8 fs in 20 fs) is within the pulse envelope, it is clear from our simulations that it is not due to a finite pulse duration effect as suggested previously.[57] It is actually the result of rapid spreading (destructive interference) of the intramolecular vibrational wave packets. That is, the intramolecular vibrations have roughly zero phase and interfere constructively at time zero (see Table III). The ~60 fs decay cannot be reproduced using intramolecular vibrations and results from solvation dynamics. This separation between intra- and intermolecular motions is possible due to the subpulse duration time-resolution in 3PEPS. For this system it provides an answer to the long standing question of how to apportion the electronic absorption width between intramolecular vibrations and solvent motions. A more detailed analysis in terms of $M(t)$ will be given in Sec. IV E.

C. Transient grating

TG signals for IR144 in the same solvents studied by 3PEPS were also measured. A typical TG signal, here for methanol as solvent, is shown in Fig. 15. As shown in Sec. III, the TG signals carry the same dynamical information as in 3PEPS in addition to the population decay of the excited electronic (S_1) state. The S_1 lifetime of IR144 in ethanol measured with phase fluorometry is ~600 ps,[91] and in the TG measurements it should appear as a ~300 ps decay, since a modulus squared of $P^{(3)}(t')$ is measured. The S_1 lifetime obtained from the TG signals in this study is ~400 ps (vide infra). Once the 200 ps lifetime component is removed from the TG signal [by multiplication by $\exp(t/\tau)$], the TG signal should reflect the same dynamical information as 3PEPS. The TG signal has a spike peaking at ~20 fs which is due to the intramolecular vibrations as well as the ultrafast solvation process.

We first fit the TG signal in the region free from the coherence spike ($T>100$ fs) using a linear prediction singular value decomposition (LP-SVD) method.[92,93] The frequencies identified by the LP-SVD are listed in Table III. The TG signals are then fitted to three exponentials (again for $T>100$ fs) while the oscillatory part from the LP-SVD fit is fixed. The results are listed in Table II(b) along with the 3PEPS data [Table II(a)]. Note that the subscripts in the time constants start from 2 to allow easy comparison with the 3PEPS data. The ~200 ps (τ_4) component found in alcohols and ethylene glycol is the lifetime component, not a reorientational relaxation, since it is more or less independent of solvent. Reorientational relaxation times are very sensitive to the solvent viscosity, while lifetimes are, in general, similar in different solvents.[94] The longest time constant in methanol is 120 ps and is considerably shorter than the ~200 ps found in other solvents. Since all parallel polarizations have been used in both 3PE and TG measurements, the reorientational motion of the chromophore will affect the signal. In particular, the TG signal should contain a decay component reflecting reorientational relaxation. The reorientation time of IR144 has not been measured, but we can estimate it from the values of similar dyes. For example, the reorientation relaxation time of HITCI in methanol is measured to be 230 ps while it is 440 ps in propanol.[94] In ethylene glycol, the reorientation time of DODCI is ~3.2 ns.[95] IR144 is larger than HITCI (or DODCI), and thus the reorientation time of the IR144 should be longer than that of HITCI. In methanol

it is plausible that the lifetime and the reorientation times are comparable. In this case the 120 ps reflects both the lifetime and the reorientation times. In the 3PE, however, the echo intensity will be affected by the reorientational motion as in TG, but the peak shift in 3PEPS may not be sensitive to the reorientational motion just as the lifetime contribution does not appear in the 3PEPS.

As in 3PEPS, the initial part of the TG signal in different solvents are indistinguishable. Only the intermediate time constants (τ_2 and τ_3) are significantly different in different solvents. The two shorter time constants from the three exponential fit of TG signals match remarkably well with the two picosecond time scales (τ_2 and τ_3) from the 3PEPS. *This clearly demonstrates that TG and 3PEPS measure the same dynamics*. Also listed, for comparison, in Table II(b) are decay time constants from TG measurements of oxazine dyes (cresyl violet and LD 690) in ethylene glycol[96]. The good agreement of the τ_2 and τ_3 time constants using different probe molecules strongly suggests that the dynamics responsible for the time constants are mostly localized in solvent coordinates.

The oscillation in the TG signal matches exactly with that in 3PEPS with one exception: It is shifted by about $+10$ fs from that in the 3PEPS. This shift is predicted in the numerical calculations in Sec. III (see Table I), and shows that the experimental measurements are consistent with the calculations. The vibrational frequencies obtained from LP-SVD fit (Table III) match closely with those from a Fourier transform (not shown) of the oscillatory part of the TG signal. The vibrations may originate from either the ground or the excited electronic states, and cannot readily be assigned to a particular electronic state. The phases of the oscillations, ϕ_i, are mostly near zero as simple wave-packet consideration predicts.[97] This results in a constructive interference at zero time, which will lead to an ultrafast decay in $M(t)$ near time zero. The prominent coherent spike is a direct manifestation of this constructive interference of the vibrational coherences.

D. Transient absorption

Figure 16 shows the TA signal for IR144 in methanol measured with parallel pump and probe polarizations. The signal is independent of the polarizations of the input pulse (magic angle and perpendicular polarizations give identical results at least for the time window shown in Fig. 16). The TA signal is fitted to a sum of three exponentials and a base line convoluted with a Gaussian. The width of the Gaussian and time zero are varied in the fit following the simulation in Sec. III E. The fit results are also listed in Table II(b). The width of the Gaussian determined from the fit is 34 fs, slightly longer than the width expected from an autocorrelation of a 20 fs pulse (28.3 fs). The time constants are similar to the values found in the 3PEPS and TG, showing that TA signal is also affected by the same dynamics measured in 3PEPS and TG. However, the 860 fs and 10 ps time constants, are strongly correlated: A shorter time constant in the range from 400 to 1200 fs fits with less than 1% increase in χ^2 with a corresponding change in the longer time constant (For example, time constants of 440 fs and 3.5 ps fit the TA signal very well.) That is, the two time constants are not well determined in the TA measurement. The coherence spike is small in the TA measurement as also expected from the simulation. Particularly in the TA signal from HITCI, the coherence spike is very small at low pump pulse intensity (<100 pJ). However, this does not mean that the initial ultrafast process does not exist in the system. As shown in Sec. III E, a subtle cancellation of the rephasing and nonrephasing response functions can hide the ultrafast dynamics seen in the 3PEPS and TG measurements, especially for a short pulse excitation.

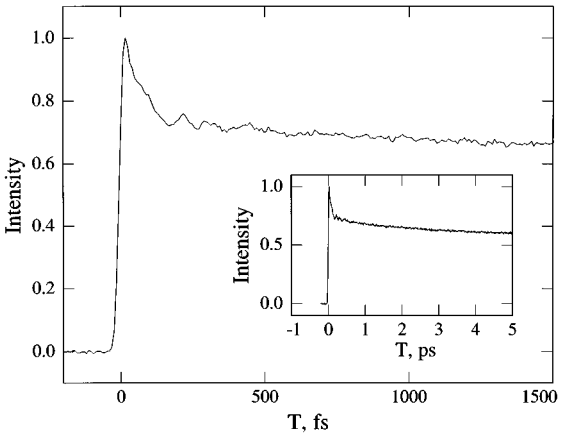

FIG. 16. TA signal of IR144 in methanol. Inset shows data out to 5 ps.

E. Obtaining $M(t)$ from the experimental data

In this section, we extract an $M(t)$ from the experimental data and demonstrate that a single $M(t)$ can be used to simulate the measured 3PEPS, TG, and TA signals. $M(t)$ contains all the relevant dynamical information on the interaction of the two electronic states and the bath, and may be used for other purposes such as a calculation of a reaction rate as shown by several authors.[98] The procedure for determining $M(t)$ is similar to the one reported previously.[66]

Based on the 3PEPS and TG measurements, the $M(t)$ may be divided into several separate contributions: intramolecular vibrational modes, $\sim$100 fs initial ultrafast dynamics (τ_1), 1–4 ps processes (τ_2), 10–100 ps processes (τ_3). Among these, only the picosecond processes (τ_2, τ_3) show significant solvent dependence in the systems studied here. The τ_2 and τ_3 processes are clearly in the slow modulation limit and they constitute Gaussian inhomogeneous broadening in the absorption spectrum. An exponential $M(t)$ with the same time constant obtained in the 3PEPS is used to account for each picosecond process. The τ_1 process is usually regarded as an inertial response of solvent, and its $M(t)$ must have zero derivative at $t=0$. The third-order measurements (3PEPS, TG, and TA) are not very sensitive to the detailed form of $M(t)$ at short times, and either a near critically damped Brownian oscillator ($\omega_i \cong 2\gamma_i$) or a Gaussian can be used.[38]

For a mathematical simplicity, we use a Gaussian for the τ_1 process. Higher-order echoes can provide a more detailed characterization of the τ_1 process.[38]

In principle, the oscillatory portion of $M(t)$ can be constructed using damped sinusoids (or underdamped Brownian oscillators[67,99]), once their frequencies, damping time constants, and displacements are known. However, there are some practical difficulties in this. Typical dye molecules used as probes have many displaced vibrations and their coupling strengths (displacements) are, in general, not known. In addition, the phases of the vibrational coherences are usually not zero, though the phase is absent in the Brownian oscillator model. We bypass these difficulties by using the experimental data directly. That is, the oscillatory component in the transient grating (TG) signal is used directly to construct a portion of $M(t)$ assuming that in the course of generating the TG signal through the response functions does not modify the intramolecular vibrational portion of $M(t)$. There are two potential problems in this method. First, if there are underdamped solvent modes in the system, they are treated as part of intramolecular vibrations. Of course this does not pose a problem in the calculation of the signals, since intramolecular vibrations and underdamped solvent modes are not distinguishable in the calculation. However, the interpretation of the results can be very different. Second, accurate measurement of the oscillatory components near zero delay is not possible. Near time zero, the oscillation is coupled with the ultrafast solvent response as well as with the coherence spike. Thus the oscillatory components of the TG signal for $T>100$ fs (Table III) are extrapolated to time zero. Specifically the TG signal away from the coherence spike ($T>100$ fs) is fitted using the linear prediction singular value decomposition (LP-SVD) method (Table III). The result from LP-SVD is extrapolated to $T=-10$ fs and shifted by $+10$ fs. The $M(t)$ determined in this way, however, has some uncertainty in its amplitude for $T<100$ fs. For a good fit to the experimental TG and 3PEPS data, a constant multiplication factor for $T<100$ fs was needed. Thus the functional form of $M(t)$ is given by

$$M(t)=A_1\ \exp[-(t/\tau_1)^2]+A_2\ \exp(-t/\tau_2)+A_3 \times\exp(-t/\tau_3)+\sum_i A_i\ \exp(-t/T_{2,i}) \times\cos(\omega_i t+\phi_i)+A_{\rm in}, \tag{11}$$

where A's are the relative coupling strengths, and $A_{\rm in}$ is a relative static (inhomogeneous) contribution. The values in Table III are used for the parameters in the damped cosinusoid term. To obtain the imaginary part of the line broadening function, $g(t)$, the reorganization energies, λ_i, are needed. For the τ_1, τ_2, and τ_3 processes in Eq. (11), the high temperature limit values, i.e., $\lambda_i=\hbar\langle\Delta\omega_i^2\rangle/2k_BT$ are used. For the oscillatory component, λ_i's for underdamped Brownian oscillators are used[67]

$$\lambda_i=\frac{\langle\Delta\omega_i^2\rangle}{2\omega_i}\cdot\left(\frac{1}{\exp(\hbar\omega_i/k_BT)-1}+\frac{1}{2}\right)^{-1}. \tag{12}$$

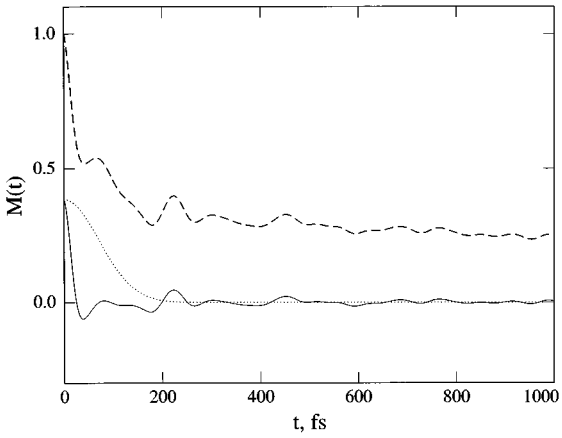

FIG. 17. The electronic transition frequency correlation function, $M(t)$, obtained from experimental 3PEPS and TG data for IR144 in methanol: Dashed line, total $M(t)$; dotted line, ultrafast Gaussian component in $M(t)$; solid line, oscillatory component arising from intramolecular vibrational motion.

Among the parameters in Eq. (11), only the coupling strengths and τ_1 are undetermined, τ_2 and τ_3 being determined directly from the 3PEPS data. As shown in Sec. III, $M(t)$ can be best determined by 3PEPS. Also 3PEPS has two advantages over TG and TA: It is almost insensitive to the imaginary part of $g(t)$, and 3PEPS calculated in the impulsive limit is very close to the 3PEPS calculated with a finite pulse duration, allowing efficient fitting of the 3PEPS data using a standard nonlinear least-square fit. The $M(t)$ determined for IR144 in methanol is shown in Fig. 17. It shows that the contributions from the initial ultrafast (τ_1) process and the vibrational contribution are very similar in

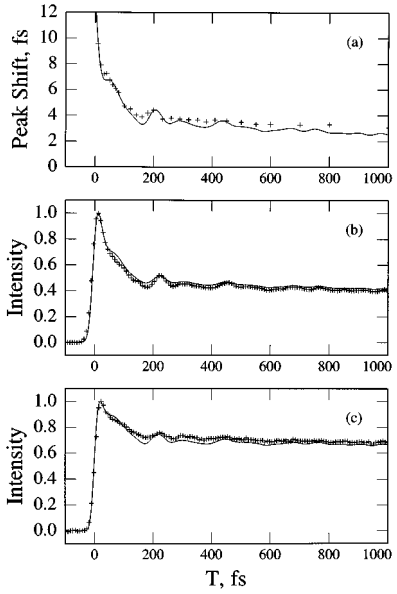

FIG. 18. Comparison of calculated and measured signals using $M(t)$ from Fig. 20. (a) 3PEPS, (b) TG, and (c) TA. A pulse duration of 20 fs and a detuning of 370 $\rm cm^{-1}$ are used in the calculated signals.

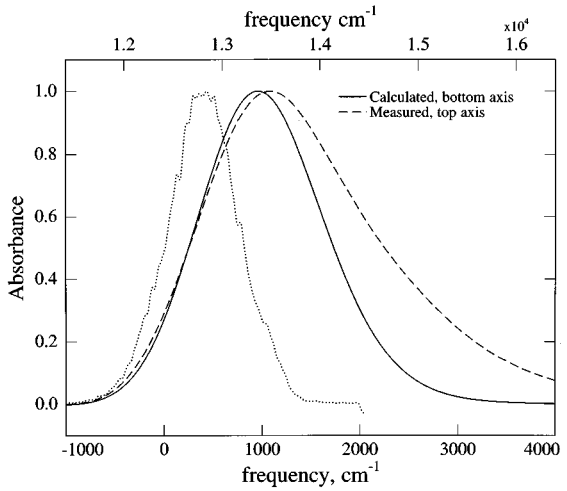

FIG. 19. Calculated (solid line) and measured (dashed line) absorption spectrum using the $M(t)$ in Fig. 17. The spectrum of the light pulses (dotted line) used in the 3PEPS, TG, and TA measurements are also shown for comparison.

this system. τ_1 is determined to be 105 fs, which is longer than the time constant obtained from the direct fit of the 3PEPS data.

Now $M(t)$, determined mostly from 3PEPS, can be used to calculate the TG and TA signals. In fact, one can calculate any linear or nonlinear spectroscopic signal once the system $M(t)$ is known. The calculated 3PEPS, TG, and TA signals using the same $M(t)$ are shown in Fig. 18 together with the experimental data. The calculated and measured signals match closely. In particular, the coherence spikes in the TG and TA signals are well reproduced. An absorption spectrum calculated from the same $M(t)$, together with the absorption spectrum of IR144 in methanol, is shown in Fig. 19. The laser pulse spectrum used in the measurement is also shown for comparison. The calculated absorption spectrum is asymmetric, and its peak is shifted by $\sim$950 cm^{-1} from zero. The calculated Stokes shift is then 2×950 cm^{-1}, and is close to the Stokes shift of IR144 in methanol ($\sim$2000 cm^{-1}). The disagreement between the calculated and measured spectra on the high frequency side probably results from the fact that the laser spectrum overlaps with the red side of the spectrum only. It is also possible that a high frequency mode was not impulsively excited and thus missed in the analysis of the TG data.

V. DISCUSSION

In Sec. III, we have shown theoretically that several third-order time domain measurements, namely, 3PEPS, TG, and TA, can give information on nuclear dynamics. We described in detail how the (solvation) dynamics is manifested in the third-order time domain measurements. In essence, the sensitivity to dynamics arises from the fact that there are two coherence periods, τ and t', separated by a population period, T, and that the correlation between the two coherence periods may be lost during T. During the coherence times, the electronic phases are determined by the transition frequency $\omega_{eg}(t)$. When the phase evolutions of the two coherence periods are correlated, the third-order polarization is different from that created when they are not correlated, which is just an FID. In a sense 3PEPS (and also TG/TA), through the rephasing term, records the difference in time evolution between the two coherence periods separated by T. Thus, even though the line broadening function $g(t)$ [see Eq.s (3) and (4)], which gives the free induction decay manifested by the linear absorption spectrum, does not show any prominent sign of dynamics, 3PEPS can pick out the dynamics occurring during the population period, T.

The main difference between the photon echo measurements and the TG/TA measurements is that the duration of the coherence periods are controllable parameters (τ actively but t' only passively) in an echo measurement while they are determined by the pulse duration in TG/TA measurements. Thus the sensitivity to dynamics is dependent on the pulse duration in TG/TA, while 3PEPS is more or less insensitive to pulse duration. Also the TA signal is less sensitive to the dynamics than TG, due to the heterodyning of the third-order polarization against the probe pulse. Using numerical simulations, we have demonstrated each technique's capability. 3PEPS is shown to be the most robust and clear measurement of the fluctuation on the optical transition frequency, $M(t)$, while *the dynamics other than population relaxation extracted from TA measurements may not represent true dynamical time scales of the system*. TG measurements can give reliable information on dynamics, although a static contribution may not be obtained from TG measurement. Also, it is difficult to obtain an accurate $M(t)$ near time zero due to the *coherence spike*.

The *coherence spike* is a conspicuous feature in both calculated and measured TG/TA signals near time zero. The coherence spike has been calculated previously in the optical Bloch model.[80,81,84,85] In the Bloch model, the coherence spike originates from the nonproperly time ordered Feynman diagrams (R_3,R_4). If one attempts to simulate a coherent spike as strong as that observed in the TG/TA experiments using only the nonproperly time-ordered terms, the parameters become physically unrealistic—the dynamics approach the Bloch limit. Of course in this case, 3PEPS (and TG/TA) cannot be reproduced. It is shown through numerical calculations that the spike arises almost entirely from the initial ultrafast decay in $M(t)$ not from the nonproperly time-ordered terms in the response functions, at least for the range of parameters used here. Thus the term *coherence spike*, not to mention *coherence artifact*, is not appropriate, since it is not a result of a coherent interaction between the pump and probe pulses.

The dynamics of polar chromophores in polar solvents shows a rather universal dynamical behavior. The dynamics occurring on systems studied here may be represented by four well separated time scales: an intramolecular vibrational component, an ultrafast ($\sim$100 fs) decay, 1$\sim$4 ps, and 10$\sim$100 ps. The intramolecular vibrations make an important contribution, but can be separated from the solvation dynamics and will not be discussed here. Of course the num-

ber of time scales really needed (or the number of actual physical processes) is somewhat arbitrary and the above three time scales represent a minimum number consistent with the experimental results.

To discuss the significance of the time scales revealed by the 3PEPS data (Table II), we first note that Cho *et al.*[77] has recently shown that the 3PEPS curve quantitatively follows $M(t)$ $[=S(t)$ in the high temperature limit, Eqs. (1) and (2)] for $T \geqslant 100$ fs. For shorter times, as the simulations presented in Table I show, the amplitude of the fastest component in $M(t)$ is overestimated, and its time scale is underestimated by fitting 3PEPS data. Thus the components τ_2 and τ_3 in Table II can be compared directly with the comprehensive fluorescence Stokes shift study of Coumarin 153 in many solvents reported by Maroncelli and co-workers.[16] The correspondence is good—for example, for IR144 in methanol, we find $\tau_2=1.4$ ps and $\tau_3=11$ ps with relative amplitudes of 1.41:1, whereas Horng *et al.*[16] obtain 3.2 and 15.3 ps with relative amplitudes of 1.14:1 for Coumarin 153 in the same solvent. In ethylene glycol, their two longest times are 5 and 32 ps with relative amplitudes of 0.59:1, whereas we obtain 3.4 and 48 ps (0.74:1). Similar levels of agreement exist for ethanol and butanol; however, in the latter solvent Horng *et al.*[16] found an additional 133 ps component which would appear static in our measurements. As the extensive analysis of Horng *et al.*[16] shows, the picosecond time scale relaxations undoubtedly arise from dielectric relaxation process and can be quantitatively predicted from frequency dependent dielectric data via the dynamical mean spherical approximation[100–102] or more sophisticated theories such as those due to Raineri *et al.*[23] or Roy and Bagchi.[22] Simulations based on detailed molecular charge distributions[28,103] imply small differences between different (large) solutes, so that exact correspondence is not necessarily to be expected between experiments using different probes. Thus, the differences seen in HITCI and IR144 in ethylene glycol in Table II seem quite reasonable.

The ultrafast component in solvation dynamics was first observed by Rosenthal *et al.*[28] in acetonitrile and methanol[29] and by Jimenez *et al.* in water.[30] Optical Kerr,[104–108] far infrared absorption spectra,[109] and a large body of simulation[18–20] and theory[21–24] also support the idea of ultrafast component arising from librational (i.e., rotational) motions and dominated by the first solvation shell. Simulations and instantaneous normal mode analyses imply that this ultrafast component is entirely Gaussian in nature and results from free (small amplitude) motions of solvent molecules that can be regarded equivalently from single molecule or collective perspectives.[21(c)] However, the normal mode analyses are currently restricted to harmonic normal modes, and as Olender and Nitzan[25] have recently pointed out, if the strongly coupled modes are coupled to a large set of other modes (i.e., in the language of gas phase spectroscopy IVR occurs) the Gaussian component may exist only on physically irrelevant time scales. In other words, in this case, very fast dynamics can still occur but it will appear dissipative (exponential) rather than reversible (Gaussian). Third-order measurements such as 3PEPS are rather insensitive to this distinction. In earlier work,[38] we used fifth-order experiments to show that the initial dynamics of HITCI in ethylene glycol are better described as Gaussian than exponential. HITCI has a significantly smaller intramolecular vibrational contribution to the dynamics than IR144, however, in Ref. 38 we did not attempt to separate intramolecular and solvent contributions to the fifth-order signals and further work along these lines is clearly desirable.

Turning to the ultrafast components in the peak shift reported in Table II, we first note that, for example, with IR144 in methanol the τ_1 of 65 fs corresponds to a Gaussian τ_{1g} [i.e., $\exp[-(t/\tau_{1g})^2]$ in $M(t)$] of 105 fs. This is in good accord with the recent simulation of Kumar and Maroncelli[103] who obtain $\tau_{1g} \sim 80$ fs for Coumarin 153 in methanol. Our results differ quantitatively from the fits of their fluorescence Stokes shift data given by Horng *et al.*,[16] which it must be noted had significantly lower time resolution than the present study. For methanol the average of the two fastest components (30 and 280 fs) given by Horng *et al.* is 98 fs. Similarly in ethanol the average is 92 fs. For butanol and ethylene glycol, however, the fastest components observed in the fluorescence data are 243 and 187 fs, respectively, whereas 3PEPS shows $\sim$100 fs components in $M(t)$ for both solvents. The amplitude of the fastest component(s) decreases with increasing size in the 1-alkanols (Table II) consistent with the fluorescence results in methanol and ethanol. However, even given that the fits in Table II overestimate the amplitude of the fastest component in $M(t)$, the overall amplitude of the ultrafast component (excluding vibrations!) is significantly larger in the echo data than in the fluorescence data.

The time scale of the ultrafast solvation component is remarkably similar in the systems studied here. IR144 in polar aprotic solvents such as acetonitrile, chloroform, and benzonitrile shows very similar time scales.[110] A very similar time scale is also found for IR144 in a room temperature glass (PMMA).[110] This latter finding is perhaps not so surprising in the light of Maroncelli's ''frozen cage'' simulation[19] or the instantaneous normal mode description of Stratt and Cho[21(c)] and Ladanyi and Stratt.[21(b)] For the systems studied here, the 100 fs component accounts for roughly half of the total solvation energy. Following the initial work of Cho *et al.*,[106] Scherer and co-workers[55] have used the spectral density obtained from optical Kerr measurements to interpret echo data. In many cases this may work well for predicting the ultrafast dynamics. Acetonitrile seems to be such a case and Ladanyi and Klein[111] have shown that the polarizability anisotropy spectral density and solvation spectral density are very similar (and both are dominated by rotational motions) as was initially guessed by Cho *et al.*[106] In general, however, the weighting factors for the bare liquid density of states may show quite different frequency dependence for different observables, and it will be interesting to explore this topic for a wide range of systems via 3PEPS measurements.

The picosecond components in TA/TG measurements have been discussed in terms of vibrational relaxation.[60,96]

The present study, however, strongly suggests that they originate from the dielectric solvation relaxation. 3PEPS measurements on a room temperature glass[110] also strongly support this view. In a 3PEPS measurement of IR144 in a glass PMMA at room temperature, no picosecond time scales were found.[110] Were they from vibrational relaxation, they would be equally present in a glass at room temperature.

VI. CONCLUDING REMARKS

The peak shift of the 3PE signal reflects the asymmetry of the signal. To be more precise, it is a measure of the difference between the signal decay on the rephasing side ($\tau>0$) and that on the nonrephasing side ($\tau<0$). Thus the shift in 3PE is a measure of the system's ability to rephase (to cause an echo), i.e., the system's degree of retained memory of its Bohr frequency after spending a time, T, in a population state. The population state includes both ground and excited electronic states. In this sense the peak shift measurement as a function of T is an indirect way of measuring $M(t)$, and it should follow $M(t)$ at least qualitatively. We have shown through numerical simulation that the 3PEPS indeed follow $M(t)$ closely. Very recently Cho *et al.*[77] have been able to show analytically that this is so. One remarkable aspect of 3PEPS is its ability to pick out dynamical information from $t=0$ even when a moderately long pulse is employed. This allows accurate separation of intramolecular underdamped oscillations and intermolecular solvation dynamics. Also unlike TG or TA measurements, which give information only on population dynamics in the impulsive limit, 3PEPS is fully responsive to solvent solute coupling in the impulsive limit. It is also very sensitive to oscillatory contributions and can pick out intramolecular vibrations which may not be easily resolvable in a TA or TG measurements. Other features that make 3PEPS attractive are its insensitivity to the population dynamics and its unique capability to pick out a static (inhomogeneous) component in $M(t)$. We will take up this in more detail elsewhere.[77,110] 3PEPS, however, is a two-dimensional technique (τ and T) and requires a longer time both for data acquisition and calculation of signal than does TA or TG.

We have shown that transient absorption (TA) and transient grating (TG) can also be used for the study on solvation dynamics. It is important to recognize that the sensitivity of the TG and TA signals to the solvation dynamics originates from the finite pulse duration. A finite field envelope provides a nonzero τ contribution to the signal, and by the same mechanism as in the echo measurement, namely the rephasing and subsequent loss of the rephasing capability by solvation, the signals become sensitive to the solvation. After removing the contribution from population relaxation, the remainder of the decay is due to the solvation dynamics. The TG measurement can be a reliable technique for the study of solvation dynamics. TA, however, may not be reliable technique for solvation studies for several reasons: It is perhaps too sensitive to the experimental conditions such as pulse duration and center wavelengths. This is due to the rising contribution from the nonrephasing (R_2) response term (in 3PEPS, R_1 determines the peak shift in the impulsive limit). Though both TG and TA suffer from the same problem, this problem is usually accentuated in TA due to the heterodyning of the third-order polarization. One way to make the TG more sensitive to the dynamics is to adjust the overlap of the first two pulses. That is, by placing a small time delay between the first two pulses in a TG experiment, it will be possible to separately pick out R_1 ($\tau>0$) or R_2 ($\tau<0$).

The applicability of the theoretical and numerical results are demonstrated experimentally. We also have presented new data on the solvation dynamics in polar protic solvents. By virtue of the subpulse duration time resolution in the 3PEPS technique the intramolecular vibrational contribution to electronic dephasing, which often obscures the intermolecular dynamics or at least hampers the interpretation, can be isolated. This allows us to resolve the ultrafast solvation process accurately. The initial ultrafast solvation dynamics occurs in ~100 fs period and is similar in time scale for the solvents studied. The amplitude of the 100 fs component in the solvation response decreases by ~30% from methanol to butanol. A strong solvent dependence is apparent on picosecond time scales. The picosecond relaxation time scales match well with fluorescence data, and predictions based on molecular models using frequency dependent dielectric data as input.

ACKNOWLEDGMENTS

We thank Minhaeng Cho for many useful discussions. Jae-Young Yu is a GAANN fellow. G.R.F. thanks the chemistry department at Cornell University for their hospitality during the period when this work was completed. This work was supported by a grant from the National Science Foundation and in part by the American Chemical Society Petroleum Research Fund.

[1] J. T. Hynes, in *Ultrafast Dynamics of Chemical Systems*, edited by J. D. Simon (Kluwer, Dordrecht, 1994), p. 345.
[2] H. Heitele, Angew. Chem. Int. Ed. Engl. **32**, 359 (1993).
[3] M. J. Weaver, Chem. Rev. **92**, 463 (1992); M. J. Weaver and G. E. McManis, Acc. Chem. Res. **23**, 294 (1990).
[4] P. J. Rossky and J. D. Simon, Nature **370**, 263 (1994).
[5] M. Watanabe, T. T. Woster, and R. W. Murray, J. Phys. Chem. **95**, 4573 (1991).
[6] P. F. Barbara and W. Jarzeba, Adv. Photochem. **15**, 1 (1990).
[7] T. J. Kang, W. Jarzeba, P. F. Barbara, and T. Fonseca, Chem. Phys. **149**, 81 (1990); K. Tominaga, G. C. Walker, T. J. Kang, P. F. Barbara, and T. Fonseca, J. Phys. Chem. **95**, 10485 (1991).
[8] J. N. Gehlen, M. Marchi, and D. Chandler, Science **263**, 499 (1994).
[9] B. B. Smith, A. Staib, and J. T. Hynes, Chem. Phys. **176**, 521 (1993).
[10] J. S. Bader, R. A. Kuharski, and D. Chandler, J. Chem. Phys. **93**, 230 (1990).
[11] H. Sumi and R. A. Marcus, J. Chem. Phys. **84**, 4894 (1986).
[12] X. Song and R. A. Marcus, J. Chem. Phys. **99**, 7768 (1993).
[13] I. Rips and J. Jortner, J. Chem. Phys. **87**, 6513 (1987).
[14] J. T. Hynes, J. Phys. Chem. **90**, 3701 (1986).
[15] J. M. Jean, R. A. Friesner, and G. R. Fleming, J. Chem. Phys. **96**, 5827 (1992); J. M. Jean, *ibid.* **101**, 10464 (1994).
[16] For a review and references, see M. L. Horng, J. Gardecki, A. Papazyan, and M. Maroncelli, J. Phys. Chem. **99**, 17311 (1995).
[17] M. Maroncelli, J. Mol. Liq. **57**, 1 (1993).
[18] M. Maroncelli and G. R. Fleming, J. Chem. Phys. **89**, 5044 (1988).
[19] M. Maroncelli, J. Chem. Phys. **94**, 2084 (1991).
[20] E. A. Carter and J. T. Hynes, J. Chem. Phys. **94**, 5961 (1991).

[21] (a) M. Cho, G. R. Fleming, S. Saito, I. Ohmine, and R. Stratt, J. Chem. Phys. **100**, 6672 (1994); (b) B. M. Ladanyi and R. M. Stratt, J. Phys. Chem. **99**, 2502 (1995); (c) R. M. Stratt and M. Cho, *ibid*. **100**, 6700 (1994).
[22] S. Roy and B. Bagchi, J. Chem. Phys. **99**, 9938 (1993).
[23] F. O. Raineri, H. Resat, B.-C. Perng, F. Hirata and H. L. Friedman, J. Chem. Phys. **100**, 1477 (1994).
[24] N. E. Shemetulskis and R. F. Loring, J. Chem. Phys. **97**, 1217 (1992).
[25] R. Olender and A. Nitzan, J. Chem. Phys. **102**, 7180 (1995).
[26] P. L. Muiño and P. R. Callis, J. Chem. Phys. **100**, 4093 (1994).
[27] B. D. Bursulaya, D. A. Zichi, and H. J. Kim, J. Phys. Chem. **99**, 10069 (1995).
[28] S. J. Rosenthal, X. L. Xie, M. Du, and G. R. Fleming, J. Chem. Phys. **95**, 4715 (1991).
[29] S. J. Rosenthal, R. Jimennez, G. R. Fleming, P. V. Kumar, and M. Maroncelli, J. Mol. Liq. **60**, 25 (1994).
[30] R. Jimenez, G. R. Fleming, P. V. Kumar, and M. Maroncelli, Nature **369**, 471 (1994).
[31] D. Bingemann and A. P. Baronavski, Chem. Phys. Lett. **201**, 153 (1993).
[32] X. Zhang, M. Kozik, N. Sutin, and J. R. Winkler, J. Am. Chem. Soc. **16**, 247 (1991).
[33] Y. Lin and C. D. Jonah, J. Phys. Chem. **97**, 295 (1993); **96**, 10119 (1992).
[34] H. Pal, Y. Nagasawa, K. Tominaga, S. Kumazaki, and K. Yoshihara, J. Chem. Phys. **102**, 7758 (1995).
[35] T. Gustavsson, G. Baldacchino, J.-C. Mialocq, and S. Pommeret, Chem. Phys. Lett. **236**, 587 (1995).
[36] F. H. Stillinger and T. A. Weber, Phys. Rev. **25**, 978 (1982); Science **225**, 983 (1984).
[37] I. Ohmine, H. Tanaka, and P. G. Wolynes, J. Chem. Phys. **89**, 5822 (1988).
[38] T. Joo, Y. Jia, and G. R. Fleming, J. Chem. Phys. **102**, 4063 (1995).
[39] In the spin-boson model, time scales and coupling strengths are characterized by means of a spectral density, $J(\omega)$. For a review see A. J. Leggett, S. Chakravarty, A. T. Dorsey, M. P. A. Fisher, A. Garg, and W. Zwerger, Rev. Mod. Phys. **59**, 1 (1987).
[40] E. L. Hahn, Phys. Rev. **80**, 580 (1950).
[41] N. A. Kurnit, I. D. Abella, and S. R. Hartmann, Phys. Rev. Lett. **13**, 567 (1964); I. D. Abella, N. A. Kurnit, and S. R. Hartmann, *ibid*. **141**, 391 (1965).
[42] For a review see J. Friedrich and D. Haarer, Angew. Chem. Int. Ed. Engl. **23**, 113 (1984).
[43] A. A. Gorokhovskii, R. K. Kaarli, and L. A. Rebane, JETP Lett. **20**, 216 (1974); B. M. Kharlamov, R. I. Personov, and L. A. Bykovskaya, Opt. Comm. **12**, 191 (1974).
[44] T. Joo and A. C. Albrecht, Chem. Phys. **176**, 233 (1993).
[45] M. Cho and G. R. Fleming, J. Phys. Chem. **98**, 3478 (1994).
[46] T. J. Kang, J. Yu, and M. Berg, J. Chem. Phys. **94**, 2413 (1991).
[47] M. T. Asaki, C.-P. Huang, D. Garvey, J. Zhou, H. C. Kapteyn, and M. M. Murnane, Opt. Lett. **18**, 977 (1993); B. Proctor and F. Wise, Appl. Phys. Lett. **62**, 470 (1993); A. Stingl, C. Spielmann, and F. Krausz, Opt. Lett. **19**, 204 (1994).
[48] S. R. Meech, A. J. Hoff, and D. A. Wiersma, Chem. Phys. Lett. **121**, 287 (1985); S. R. Meech, A. J. Hoff, and D. A. Wiersma, Proc. Natl. Acad. Sci. USA **83**, 9464 (1986).
[49] A. M. Weiner, S. De Silvestri, and E. P. Ippen, J. Opt. Soc. Am. B **2**, 654 (1985).
[50] P. C. Becker, H. L. Fragnito, J. Y. Bigot, C. H. Brito Cruz, R. L. Fork, and C. V. Shank, Phys. Rev. Lett. **63**, 505 (1989).
[51] J.-Y. Bigot, M. T. Portella, R. W. Schoenlein, C. J. Bardeen, A. Migus, and C. V. Shank, Phys. Rev. Lett. **66**, 1138 (1991).
[52] E. T. J. Nibbering, D. A. Wiersma, and K. Duppen, Phys. Rev. Lett. **66**, 2464 (1991).
[53] W. P. de Boeij, M. S. Pshenichnikov, K. Duppen, and D. A. Wiersma, Chem. Phys. Lett. **224**, 243 (1994).
[54] C. J. Bardeen and C. V. Shank, Chem. Phys. Lett. **203**, 535 (1993); **226**, 310 (1994).
[55] P. Vöhringer, D. C. Arnett, R. A. Westervelt, M. J. Feldstein, and N. F. Scherer, J. Chem. Phys. **102**, 4027 (1995).
[56] P. Vöhringer, D. C. Arnett, T.-S. Yang, and N. F. Scherer Chem. Phys. Lett. **237**, 387 (1995); M. S. Pshenichnikov, K. Duppen, and D. A. Wiersma, Phys. Rev. Lett. **74**, 674 (1995).
[57] W. P. de Boeij, M. S. Pshenichnikov, and D. A. Wiersma, Chem. Phys. Lett. **238**, 1 (1995).
[58] Optical pure dephasing time is not well defined in liquid, since it is dependent on the measurement time scale. The time dependence originates from the finite time scale in $M(t)$ as shown in Sec. III.
[59] M. Cho, N. F. Scherer, G. R. Fleming, and S. Mukamel, J. Chem. Phys. **96**, 5618 (1992); M. Cho and G. R. Fleming, *ibid*. **98**, 2848 (1993).
[60] S. Savikhin and W. S. Struve, Biophys. J. **67**, 2002 (1994).
[61] S. Y. Goldberg, E. Bart, A. Meltsin, B. D. Fainberg, and D. Huppert, Chem. Phys. **183**, 217 (1994). For a recent review of transient grating method, see F.-W. Deeg, in *Dynamics During Spectroscopic Transitions*, edited by E. Lippert and J. D. Macomber (Springer, New York, 1995), p. 456.
[62] A. B. Myers, J. Opt. Soc. Am. B **7**, 1665 (1990); M. K. Lawless and R. A. Mathies, J. Chem. Phys. **96**, 8037 (1992); E. T. J. Nibbering, D. A. Wiersma, and K. Duppen, Chem. Phys. **183**, 167 (1994).
[63] E. W. Castner, Jr., M. Maroncelli, and G. R. Fleming, J. Chem. Phys. **86**, 1090 (1987).
[64] B. Bagchi, D. W. Oxtoby, and G. R. Fleming, Chem. Phys. **86**, 257 (1984).
[65] Y. J. Yan and S. Mukamel, Phys. Rev. A **41**, 6485 (1990).
[66] T. Joo, Y. Jia, J.-Y. Yu, D. M. Jonas, and G. R. Fleming, J. Phys. Chem. **100**, 2399 (1996).
[67] (a) S. Mukamel, *Principles of Nonlinear Optical Spectroscopy* (Oxford, New York, 1995); (b) S. Mukamel, Annu. Rev. Phys. Chem. **41**, 647 (1990); (c) Y. J. Yan and S. Mukamel, J. Chem. Phys. **94**, 179 (1991).
[68] E. Hanamura, J. Phys. Soc. Jpn. **52**, 2258 (1983).
[69] B. D. Fainberg, Opt. Spectrosc. **55**, 669 (1983).
[70] R. Kubo, Adv. Chem. Phys. **15**, 101 (1969).
[71] When the excited state population relaxes to a third state such as a triplet state T_1, it decays by the ground state recovery time, not by the decay time to T_1.
[72] N. F. Scherer, D. M. Jonas, and G. R. Fleming, J. Chem. Phys. **99**, 153 (1993).
[73] The change in the environment during time T initiated by an electronic transition causes the energy change of both the electronic excited and the electronic ground states.
[74] L. J. Root, J. Chem. Phys. **93**, 4364 (1990).
[75] R. F. Loring and S. Mukamel, Chem. Phys. Lett. **114**, 426 (1985).
[76] $\tau_c = \int_0^\infty M(t)dt$.
[77] M. Cho, J.-Y. Yu, T. Joo, and G. R. Fleming, J. Phys. Chem. (in press).
[78] L. E. Fried, N. Bernstein, and S. Mukamel, Phys. Rev. Lett. **68**, 1842 (1992).
[79] E. W. Castner, Jr., Y. J. Chang, Y. C. Chu, and G. E. Walrafen, J. Chem. Phys. **102**, 653 (1994).
[80] M. W. Balk and G. R. Fleming, J. Chem. Phys. **83**, 4300 (1985).
[81] (a) P. Cong, H. P. Deuel, and J. D. Simon, Chem. Phys. Lett. **212**, 367 (1993); (b) P. Cong, Y. J. Yan, H. P. Deuel, and J. D. Simon, J. Chem. Phys. **100**, 7855 (1993).
[82] G. Stock and W. Domcke, Phys. Rev. A **45**, 3032 (1992).
[83] Y. R. Shen, *The Principles of Nonlinear Optics* (Wiley, New York, 1984).
[84] I. A. Walmsley, M. Mitsunaga, and C. L. Tang, Phys. Rev. A **38**, 4681 (1988).
[85] M. Chachisvilis, H. Fidder, and V. Sundström, Chem. Phys. Lett. **234**, 141 (1995).
[86] E. Gaizauskas and L. Valkunas, Opt. Comm. **109**, 75 (1994).
[87] W. B. Bosma, Y. J. Yan, and S. Mukamel Phys. Rev. A **42**, 6920 (1990).
[88] K. Leo, M. Wegener, J. Shah, D. S. Chemla, E. O. Göbel, T. C. Damen, S. Schmitt-Rink, and W. Schäfer, Phys. Rev. Lett. **65**, 1340 (1990).
[89] M. van Burgel, D. A. Wiersma, and K. Duppen, J. Chem. Phys. **102**, 20 (1995).
[90] S. Wu, X.-C. Zhang, and R. L. Fork, Appl. Phys. Lett. **61**, 919 (1992).
[91] R. B. Thompson, J. K. Frisoli, and J. R. Lakowicz, Anal. Chem. **64**, 2075 (1992).
[92] H. Barkhuijsen, R. de Beer, W. M. M. J. Bovée, and D. van Ormondt, J. Mag. Res. **61**, 465 (1985).
[93] F. W. Wise, M. J. Rosker, G. L. Millhauser, and C. L. Tang, IEEE J. Quant. Elect. **QE-23**, 1116 (1987).
[94] G. S. Beddard, T. Doust, and G. Porter, Chem. Phys. **61**, 17 (1981).
[95] P. A. Anfinrud and W. S. Struve, J. Chem. Phys. **87**, 4256 (1987).
[96] T. Joo and A. C. Albrecht, Chem. Phys. **173**, 171 (1993).
[97] D. M. Jonas, S. E. Bradforth, S. A. Passino, and G. R. Fleming, J. Phys. Chem. **99**, 2594 (1995).
[98] S. Creighton, J. K. Hwang, A. Warshel, W. W. Parson, and J. Norris, Biochemistry **27**, 774 (1988); R. Egger and C. H. Mak, J. Phys. Chem. **98**,

9903 (1994); M. Cho and R. J. Silbey, J. Chem. Phys. **103**, 595 (1995).
[99] W. Bosma, Y. J. Yan, and S. Mukamel, Phys. Rev. A **42**, 6920 (1990).
[100] P. G. Wolynes, J. Chem. Phys. **86**, 5133 (1987).
[101] I. Rips, J. Klafter, and J. Jortner, J. Chem. Phys. **89**, 4288 (1988).
[102] M. Maroncelli and G. R. Fleming, J. Chem. Phys. **89**, 875 (1988).
[103] P. V. Kumar and M. Maroncelli, J. Chem. Phys. **103**, 3088 (1995).
[104] D. McMorrow, W. T. Lotshaw, and G. A. Kenney-Wallace, IEEE J. Quant. Elec. **QE-24**, 443 (1988); D. McMorrow and W. T. Lotshaw, J. Phys. Chem. **95**, 10395 (1991); D. McMorrow and W. T. Lotshaw, Chem. Phys. Lett. **201**, 369 (1993).
[105] S. Ruhman, B. Kohler, A. G. Joly, and K. A. Nelson, J. Chem. Phys. **141**, 16 (1987); S. Ruhman, A. G. Joly, and K. A. Nelson, IEEE J. Quan. Elec. **QE-24**, 470 (1988); S. Ruhman and K. A. Nelson, J. Chem. Phys. **94**, 859 (1991).
[106] M. Cho, M. Du, N. F. Scherer, L. D. Ziegler, and G. R. Fleming, J. Chem. Phys. **96**, 5033 (1992).
[107] J. Etchepare, G. Frillon, G. Hamoniaux, and A. Orszag, Opt. Comm. **63**, 329 (1987).
[108] Y. J. Chang and E. W. Castner, Jr., J. Chem. Phys. **99**, 113 (1993).
[109] For example, see G. J. Davies and M. Evans, J. Chem. Soc. Faraday II **72**, 1194 (1975).
[110] Y. Nagasawa, S. Passino, T. Joo, and G. R. Fleming (in preparation).
[111] B. M. Ladanyi and S. Klein (private communication).
[112] D. Lee and A. C. Albrecht, in *Advances in Infrared and Raman Spectroscopy*, edited by R. J. Clark and R. E. Hester (Wiley Heyden, New York, 1985), Vol. 12.
[113] S. Y. Yee, T. K. Gustafson, S. A. J. Druet, and J.-P. E. Taran, Opt. Comm. **23**, 1 (1977).